Available online at www.sciencedirect.com

ScienceDirect

journal homepage: http://www.elsevier.com/locate/acme

Original Research Article

Thermo-magneto-elasticity analysis of variable thickness annular FGM plates with asymmetric shear and normal loads and non-uniform elastic foundations

Ahmad Behravan Rad, Mohammad Shariyat *

Faculty of Mechanical Engineering, K.N. Toosi University of Technology, Tehran, Iran

ARTICLE INFO

Article history:
Received 14 August 2015
Accepted 13 February 2016
Available online 11 March 2016

Keywords:
Non-uniform thermo-magneto-mechanical loads
Thickness variability
Functionally graded annular plate
Non-uniform elastic foundation
Lorentz force

ABSTRACT

In the present research, a semi-analytical three-dimensional solution is developed for transversely graded annular/circular plates resting on non-uniform elastic foundations and subjected to magnetic and thermal fluxes and non-uniform and asymmetric mechanical loads. Thickness of the plate may vary exponentially along the radial direction and the inner and outer edges are restrained. All the thermal, magnetic, and elastic properties are assumed to vary in the transverse direction. Transverse distribution of the temperature is determined analytically for both the specified transverse temperature gradient and specified heat flux thermal conditions. Dependencies of the solution on the radial and transverse coordinates are determined through solving the resulting governing equations by using the differential quadrature and state space approaches in the radial and transverse directions, respectively. Effects of the material heterogeneity, thermal and mechanical boundary conditions, thickness variability, coefficients of the elastic foundation, shear to normal loads ratio, and magnetic field intensity are investigated comprehensively, through a parametric study. Results reveal that complex interactions may be observed among the elastic, thermal, and magnetic responses.

1. Introduction

Stationary and rotating annular plates have extensively been used in various mechanical, electrical, and mechatronic assemblies. These plates may generally be prone to uniform or non-uniform mechanical, thermal, and/or magnetic loads and fabricated from homogeneous, heterogeneous [1,2] or even smart [3] materials and supported by foundations constructed from deformable materials. A disk of an electrical clutch/brake of a machine tool or passenger car is a typical annular plate that may be manufactured in a tapered form (variable thickness) and is subjected to a magnetic actuation, thermal loads (due to slippage of the friction disk through

* *Corresponding author at*: Center of Excellence in Smart Structures and Dynamical System, Faculty of Mechanical Engineering, K.N. Toosi University of Technology, Tehran 19991-43344, Iran. Tel.: +98 9122727199; fax: +98 21 88674748.
E-mail addresses: behravanrad@gmail.com (A. Behravan Rad), m_shariyat@yahoo.com, shariyat@kntu.ac.ir (M. Shariyat).
URL: http://wp.kntu.ac.ir/shariyat/publications.html
http://dx.doi.org/10.1016/j.acme.2016.02.006

engagement), and normal and shear mechanical tractions. Using ceramic coated or transversely graded annular plates or discs, may postpone formation of the hot spot and overheat phenomena and distortion due to severe thermal stresses during the power transmission.

Some researchers have studied one-dimensional thermo-mechanical stresses of radially graded discs undergoing radial loads. Nie and Batra [4] analyzed axisymmetric deformations of a variable thickness radially graded rotating disk. A steady thermoelastic analysis of a rotating radially graded hollow circular disk subjected to pure radial temperature gradient was made by Peng and Li [5]. Thermoelastic stress distributions of rotating radially graded disks with non-uniform thickness were determined by Hassani et al. [6].

While some thermoelastic analyses of the circular/annular plates have been performed based on the first-order plate theory [7,8,1,9,10], the exact results can only be obtained through using the three-dimensional theory of elasticity [11–13]. Wang et al. [14] presented a 3D analysis for axisymmetric bending of the functionally graded circular plates. Shariyat and Mohammadjani [15,16] studied 3D stress fields of spinning thick bidirectional functionally graded annular plates with non-uniform tractions and non-uniform elastic foundations. Behravan Rad [17] conducted a static analysis for exponentially graded circular plates resting on elastic foundations. Behravan Rad and Alibeigloo [18] investigated static axisymmetric behavior of two directional FG circular plates resting on elastic foundations. Behravan Rad [19] and Behravan Rad and Shariyat [20] analyzed respectively, variable thickness circular and uniform thickness annular functionally graded plates subjected to axisymmetric transverse and shear tractions and resting on non-uniform elastic foundations.

Numerous researches have analyzed multilayered circular plates subject to magneto-electro-mechanical loads. Pan [21] investigated static magneto-electro-elastic characteristics of the multilayered plates. Wang et al. [22] developed three-dimensional state vector equations for the orthotropic magneto-electro-elastic multilayered media. Lage et al. [23] used a layerwise partial mixed finite element method for behavior analysis of the magneto-electro-elastic plates. Alaimo et al. [24] and Razavi and Shooshtari [25] respectively, accomplished static and free vibration analyses of the magneto-electro-elastic multilayered plates, based on the first-order shear-deformation plate theory.

Magneto-electro-elastic behavior analysis of the functionally graded circular/annular plates was the motivation for some of the researches. Bhangale and Ganesan [26] proposed solutions for static analysis of functionally graded and layered magneto–electro-elastic plates. Pan and Han [27] presented an exact solution for multilayered rectangular plates made of functionally graded anisotropic magneto-electro-elastic materials. Jiangyi et al. [28] employed the state-space method to evaluate modal contents of the exponentially graded magneto-electro-elastic plates. Analytical axisymmetric response analysis of functionally graded magneto–electro-elastic circular plates under uniform loads was accomplished by Li et al. [29]. Free vibration of a functionally graded piezoelectric circular plate placed in a uniform magnetic field was investigated by Dai et al. [30]. Recently, Behravan Rad and Shariyat [31] presented a 3D magneto-elastic analysis for asymmetric variable thickness porous FGM circular plates with non-uniform tractions and Kerr elastic foundations.

Limited researches may be found in literature on thermo-magneto-elastic analysis of the circular/annular functionally graded plates. Ghorbanpour Arani et al. [32] studied stresses and displacements of a radially graded piezo-magnetic rotating disk under steady thermomechanical loads. Zenkour [33] investigated axisymmetric magneto-thermo-elastic response of a radially graded annular disk subjected to a non-uniform thermal load in a magnetic field. Li et al. [34] studied axisymmetric thermo-magneto-electro-elastic behavior of heterogeneous circular plates subjected to uniform thermal loadings on their boundaries.

In the present paper, it is intended to develop a three-dimensional thermo-magneto-elasticity solution for stress and displacement analysis of variable thickness functionally graded annular/circular plates on non-uniform elastic foundations and edge supports, subjected to non-uniform shear and normal tractions and thermal and magnetic loads. While the temperature distribution is determined analytically, a combination of the differential quadrature and state space vector techniques are employed to determine the displacement and stress components.

Novelties of the present research in comparison to the recently published work of the authors [31] are:

(i) Proposing a semi-analytical solution that is adequate for the annular (variable thickness) FGM plates, based on a 3D formulation.
(ii) Including the thermal effects (in addition to the magnetic actuation).
(iii) Employing analytical solutions associated with the specified heat flux and transverse temperature gradient thermal boundary conditions.
(iv) Considering the complex interactions among the lateral and radial displacement components, thermal effects, the induced electromagnetic quantities, and the elastic foundation. In the limited available researches, the thermo-magneto-elastic analyses have mainly been performed through 1D formulations; so that these interactions cannot be noted adequately.

2. The thermo-magneto-elasticity equations of the annular plate

2.1. *Description of the geometry, material heterogeneity, elastic foundation, and loads*

A schematic of the considered transversely graded annular plate is shown in Fig. 1 along with the employed cylindrical coordinate system (r, θ, z) whose origin is located at the center of the bottom plane of the plate. In addition to the non-uniform mechanical loads, the plate is subjected to thermal and magnetic loads. Outer and inner radii of the plate are denoted by a and b, respectively. Spatial variations of the elasticity modulus (E), thermal expansion coefficient (α), thermal conductivity coefficient (κ), and magnetic permeability (μ) may be described as:

$$E(z) = E_0 e^{n_1(z/h)} \tag{1}$$

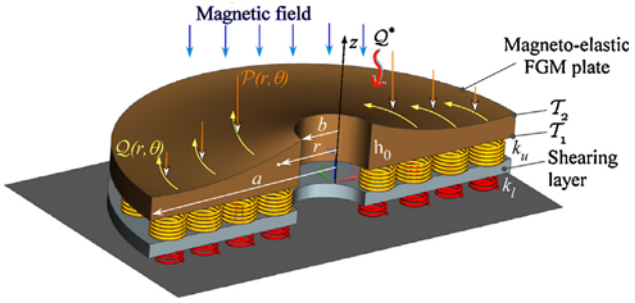

Fig. 1 – Geometry and coordinate system of the variable thickness FGM annular plate with non-uniform normal and shear tractions and thermal and magnetic fields, on a non-uniform elastic foundation.

$$\alpha(z) = \alpha_0 e^{n_2(z/h)} \tag{2}$$

$$\kappa(z) = \kappa_0 e^{n_3(z/h)} \tag{3}$$

$$\mu(z) = \mu_0 e^{n_4(z/h)} \tag{4}$$

where the quantities with subscript 0 are associated with the bottom layer of the plate. n_1, n_2, n_3 and n_4 are the heterogeneity exponents. In many applications one may use the exponential decay of the matrix phase to reach the pure stiffer/thougher phase instead using a coating (i.e., instead of using a discreetly graded material).

Thickness of the plate is assumed to vary as follows in the radial direction [35]:

$$h(r) = h_o e^{n_5\left(\frac{r-b}{a-b}\right)^2} \tag{5}$$

The bottom surface of the plate is flat and supported by the elastic foundation.

The plate is subjected to non-uniform shear and normal tractions that vary in the radial and circumferential directions according to:

$$\mathcal{P}(r,\theta) = \mathcal{P}_0\left[1 + \mathcal{A}_1\left(\frac{r-b}{a-b}\right) + \mathcal{A}_2\left(\frac{r-b}{a-b}\right)^2\right]\cos\theta \tag{6}$$

$$\mathcal{Q}(r,\theta) = \mathcal{Q}_0\left[1 + \mathcal{B}_1\left(\frac{r-b}{a-b}\right) + \mathcal{B}_2\left(\frac{r-b}{a-b}\right)^2\right]\cos\theta \tag{7}$$

where $\mathcal{P}_0$ and $\mathcal{Q}_0$ are magnitudes of the normal and shear tractions at the inner boundary of the top surface, and $\mathcal{A}_1$, $\mathcal{A}_2$, $\mathcal{B}_1$, and $\mathcal{B}_2$ are loading parameters. Indeed, each function (e.g., variations of the tractions) may be expanded trough Fourier series. By considering cosine functions for interpretation of the circumferential variations of the tractions, a plane of symmetry is considered implicitly; a fact that may be justified for several applications. Solutions corresponding to each individual cosine term of the Fourier series may be derived based on the present research. Hence, solutions to the more complicated loading conditions may be found through summing up the solutions associated with the distinct cosine terms of the Fourier series. On the other hand, in many situations, radial variations of the normal and shear tractions may be approximated by a parabolic function (in terms of the dimensionless radius).

The employed general hybrid Kerr foundation model includes a shear mid-layer whose stiffness is denoted by T and upper and lower elastic layers with stiffnesses k_u and k_l, respectively (Fig. 1). The distributed traction exerted by the elastic foundation on the bottom surface of the plate can be expressed as:

$$\mathcal{P}_s - \left(\frac{T}{k_l + k_u}\right)\nabla^2\mathcal{P}_s = \left(\frac{k_l k_u}{k_l + k_u}\right)w - \left(\frac{Tk_u}{k_l + k_u}\right)\nabla^2 w \tag{8}$$

where $\nabla^2 = \frac{\partial^2}{\partial r^2} + \frac{1}{r}\frac{\partial}{\partial r} + \frac{1}{r^2}\frac{\partial^2}{\partial\theta^2}$.

The interface pressure between the plate and the non-uniform Kerr foundation may be expressed mathematically as follows

$$\begin{aligned}\mathcal{S} - \frac{1}{r}\frac{\partial}{\partial r}\left(r\frac{T}{k_l + k_u}\mathcal{S}_{,r}\right) - \frac{1}{r^2}\frac{\partial}{\partial\theta}\left(\frac{T}{k_l + k_u}\mathcal{S}_{,\theta}\right)\\ = \left(\frac{k_l k_u}{k_l + k_u}\right)w - \frac{1}{r}\frac{\partial}{\partial r}\left(r\frac{Tk_u}{k_l + k_u}w_{,r}\right) - \frac{1}{r^2}\frac{\partial}{\partial\theta}\left(\frac{Tk_u}{k_l + k_u}w_{,\theta}\right)\end{aligned} \tag{9}$$

where $\mathcal{S}$ denotes the foundation reaction per unit area and w is the lateral deflection of the bottom surface of the plate.

It is assumed that, the hybrid elastic foundation is perfect, frictionless, perfectly attached to the plate, isotropic ($T_r = T_\theta = T$), radially graded, and periodically distributed in the circumferential direction. Therefore, distributions of the k_l, T, and k_u coefficients of the elastic foundation may be considered as:

$$\begin{aligned}k_l(r,\theta) = k_{l0}e^{f_1\left(\frac{r-b}{a-b}\right)}\cos\theta, \quad T(r,\theta) = T_0 e^{f_2\left(\frac{r-b}{a-b}\right)}\cos\theta, \quad k_u(r,\theta)\\ = k_{u0}e^{f_3\left(\frac{r-b}{a-b}\right)}\cos\theta\end{aligned} \tag{10}$$

where quantities with "0" subscript are associated with the inner boundary of the bottom surface of the plate and f_1, f_2, f_3 are exponents of variations of the foundation coefficient.

2.2. *Derivation of the governing equations*

According to the 3D theory of elasticity, the equilibrium equations may be interpreted in terms of variations of the stress components as follows, neglecting the gravitational body forces:

$$\begin{aligned}&\sigma_{r,r} + r^{-1}\tau_{r\theta,\theta} + \tau_{rz,z} + r^{-1}(\sigma_r - \sigma_\theta) + f_r = 0\\ &\tau_{r\theta,r} + r^{-1}\sigma_{\theta,\theta} + \tau_{\theta z,z} + 2r^{-1}\tau_{r\theta} = 0\\ &\tau_{rz,r} + r^{-1}\tau_{\theta z,\theta} + \sigma_{z,z} + r^{-1}\tau_{rz} = 0\end{aligned} \tag{11}$$

where σ_r, σ_θ, σ_z, τ_{rz}, $\tau_{\theta z}$, and $\tau_{r\theta}$ are the stress components, f_r is Lorentz's body force and the comma symbol denotes a partial differentiation with respect to the indicated variable.

Denoting the radial, circumferential, and axial displacement components by u, v, and w, respectively, the strain-displacement relations may be written as

$$\begin{aligned}&\epsilon_r = u(r,\theta,z)_{,r}\\ &\epsilon_\theta = r^{-1}v(r,\theta,z)_{,\theta} + r^{-1}u\\ &\epsilon_z = w(r,\theta,z)_{,z}\\ &\gamma_{rz} = u(r,\theta,z)_{,z} + w(r,\theta,z)_{,r}\\ &\gamma_{\theta z} = r^{-1}w(r,\theta,z)_{,\theta} + v(r,\theta,z)_{,z}\\ &\gamma_{r\theta} = r^{-1}u(r,\theta,z)_{,\theta} + v(r,\theta,z)_{,r} - r^{-1}v(r,\theta,z)\end{aligned} \tag{12}$$

where ε_r, ε_θ, ε_z, γ_{rz}, $\gamma_{\theta z}$, and $\gamma_{r\theta}$ are the normal and shear strain components, respectively; so that the three-dimensional

thermoelastic constitutive relations in terms of the displacement components become:

$$\begin{aligned}
\sigma_r &= \frac{E(z)}{(1+\nu)(1-2\nu)}[(1-\nu)u(r,\theta,z)_{,r} + \nu r^{-1}(v(r,\theta,z)_{,\theta} + u(r,\theta,z)) + \nu w(r,\theta,z)_{,z}] - \frac{E(z)\alpha(z)}{1-2\nu}\mathcal{T}(z)\\
\sigma_\theta &= \frac{E(z)}{(1+\nu)(1-2\nu)}[\nu u(r,\theta,z)_{,r} + (1-\nu)r^{-1}u(r,\theta,z) + \nu w(r,\theta,z)_{,z}] - \frac{E(z)\alpha(z)}{1-2\nu}\mathcal{T}(z)\\
\sigma_z &= \frac{E(z)}{(1+\nu)(1-2\nu)}[\nu u(r,\theta,z)_{,r} + \nu r^{-1}u(r,\theta,z) + (1-\nu)w(r,\theta,z)_{,z}] - \frac{E(z)\alpha(z)}{1-2\nu}\mathcal{T}(z)\\
\tau_{rz} &= \frac{E(z)}{2(1+\nu)}[u(r,\theta,z)_{,z} + w(r,\theta,z)_{,r}]\\
\tau_{\theta z} &= \frac{E(z)}{2(1+\nu)}[r^{-1}w(r,\theta,z)_{,\theta} + v(r,\theta,z)_{,z}]\\
\tau_{r\theta} &= \frac{E(z)}{2(1+\nu)}[v(r,\theta,z)_{,r} - r^{-1}v(r,\theta,z) + r^{-1}u(r,\theta,z)_{,\theta}]
\end{aligned} \tag{13}$$

where $\mathcal{T}$ is the temperature increase with respect to a stress-free state.

Based on the definition of the external mechanical loads in Eqs. (6) and (7) and the constitutive equation (13), the consistent mechanical displacement and stress fields become:

$$\begin{aligned}
&u(r,\theta,z) = u(r,z)\cos\theta, \quad v(r,\theta,z) = v(r,z)\sin\theta, \quad w(r,\theta,z) = w(r,z)\cos\theta\\
&\sigma_r(r,\theta,z,n_1,n_2) = \sigma_r(r,z,n_1,n_2)\cos\theta, \quad \sigma_\theta(r,\theta,z,n_1,n_2) = \sigma_\theta(r,z,n_1,n_2)\cos\theta,\\
&\sigma_z(r,\theta,z,n_1,n_2) = \sigma_z(r,z,n_1,n_2)\cos\theta, \quad \tau_{rz}(r,\theta,z,n_1) = \tau_{rz}(r,z,n_1)\cos\theta,\\
&\tau_{\theta z}(r,\theta,z,n_1) = \tau_{\theta z}(r,z,n_1)\sin\theta, \quad \tau_{r\theta}(r,\theta,z,n_1) = \tau_{r\theta}(r,z,n_1)\sin\theta
\end{aligned} \tag{14}$$

Denoting the heat flux by $\mathcal{Q}^*$ (Fig. 1), the steady transverse distribution of the temperature obeys:

$$\mathcal{Q}^*_{,z} = -[\kappa(z)\mathcal{T}_{,z}]_{,z} = 0 \tag{15}$$

Maxwell's electrodynamics equations of the perfectly conducting elastic body may be introduced as [30]

$$\begin{aligned}
&\mathcal{J} = \nabla\times\mathbf{h}, \quad \nabla\times\mathbf{e} = -\mu(z)\frac{\partial\mathbf{h}}{\partial t}, \quad \nabla\cdot\mathbf{h} = 0, \quad \mathbf{e}\\
&= -\mu(z)(\dot{\delta}\times\mathcal{H}), \quad \mathbf{h} = \nabla\times(\delta\times\mathcal{H})
\end{aligned} \tag{16}$$

where **J** is the electric current density vector, **e** is perturbation of the electric field vector, **h** is perturbation of the magnetic field vector, **δ** is the displacement vector, and $\mathcal{H}$ is the magnetic intensity vector, respectively.

Lorentz's force can be determined from [30,36]

$$\begin{aligned}
\mathbf{f} &= q\mathbf{V}\times\mathbf{B} = \mathcal{J}\times\mu\mathbf{h} = \mu\mathcal{J}\times\mathbf{h}\\
&= \mu\{\nabla\times[\nabla\times(\delta\times\mathcal{H})]\}\times\nabla\times(\delta\times\mathcal{H})
\end{aligned} \tag{17}$$

If $\mathcal{H} = \mathcal{H}(0,0,H_z)$, one has:

$$\begin{aligned}
&\delta = (u,0,0), \quad \mathcal{J} = (0,-h_{z,r},0), \quad \mathbf{h} = (0,0,h_z),\\
&\mathbf{e} = -\mu(z)(0,H_z\dot{u},0), \quad h_z = -H_z\left(u_{,r} + \frac{u}{r}\right)
\end{aligned} \tag{18}$$

Therefore, Maxwell's electromagnetic stress τ_z may be defined as [37]

$$\tau_{ij} = \mu(h_iH_j + h_jH_i - h_kH_k\delta_{ij}) \Rightarrow \tau_z = \mu(z)H_z^2\left(u_{,r} + \frac{u}{r}\right) \tag{19}$$

where δ_{ij} is the Kronecker delta and magnitude of Lorentz's force f_r is [24,30]

$$f_r = \mu(z)(\mathcal{J}\times\mathcal{H}) \Rightarrow f_r = \mu(z)H_z^2\frac{\partial}{\partial r}\left(u_{,r} + \frac{u}{r}\right) \equiv \tau_{z,r} \tag{20}$$

To present more general results, the following non-dimensional quantities are defined:

$$\begin{aligned}
&U = \frac{u(r,\theta,z)}{h(r)}, \quad V = \frac{v(r,\theta,z)}{h(r)}, \quad W = \frac{w(r,\theta,z)}{h(r)}, \quad \eta = \frac{r}{a}, \quad s = \frac{h_0}{a}, \quad \xi = \frac{z}{h(r)}, \quad 0\le\xi,\eta\le 1\\
&\sigma_\eta = \frac{\sigma_r}{\Sigma}, \quad \sigma_\Theta = \frac{\sigma_\theta}{\Sigma}, \quad \sigma_\xi = \frac{\sigma_z}{\Sigma}, \quad \tau_{\eta\xi} = \frac{\tau_{rz}}{\Sigma}, \quad \tau_{\Theta\xi} = \frac{\tau_{\theta z}}{\Sigma}, \quad \tau_{\eta\Theta} = \frac{\tau_{r\theta}}{\Sigma}, \quad \tau_m = \frac{\tau_z}{\Sigma}, \quad \Sigma = 1 \text{ GPa},\\
&\mu_b = \frac{2\mu_0(1+\nu)H_z^2}{E_0}, \quad h_z^* = \frac{h_z}{H_z}, \quad \overline{\mathcal{T}} = \alpha_1\mathcal{T}, \quad \alpha_1 = 10^{-6}\ \text{C}^{-1}.
\end{aligned} \tag{21}$$

Based on Eqs. (11), (13), (14) and (21), the normalized form of the governing equations in terms of the displacement components and temperature become:

$$
\begin{aligned}
U_{,\xi\xi} &= s^2\beta_1^2\left\{-\frac{2(1-\nu)}{1-2\nu}\left[U_{,\eta\eta}+\left(\frac{1}{\eta}+2\beta_2\right)U_{,\eta}+\left(\frac{\beta_2}{\eta}+\beta_3\right)U\right]+\frac{3-4\nu}{1-2\nu}\frac{U}{\eta^2}-\frac{1}{(1-2\nu)\eta}(V_{,\eta}+\beta_2 V)+\frac{3-4\nu}{1-2\nu}\frac{V}{\eta^2}\right\}\\
&\quad -s\beta_1\left\{n_1(W_{,\eta}+\beta_2 W)-\frac{1}{1-2\nu}(W_{,\eta\xi}+\beta_2 W_{,\xi})\right\}-n_1U_{,\xi}-\mu_b s^2\beta_1^2\left[U_{,\eta\eta}+\left(\frac{1}{\eta}+2\beta_2\right)U_{,\eta}+\left(\frac{\beta_2}{\eta}+\beta_3-\frac{1}{\eta^2}\right)U\right]\\
V_{,\xi\xi} &= s^2\beta_1^2\left\{\frac{1}{(1-2\nu)\eta}(U_{,\eta}+\beta_2 U)+\frac{3-4\nu}{(1-2\nu)}\frac{U}{\eta^2}+\frac{3-4\nu}{(1-2\nu)}\frac{V}{\eta^2}-\left[V_{,\eta\eta}+\left(2\beta_2+\frac{1}{\eta}\right)V_{,\eta}+(\beta_2+\beta_3)V\right]\right\}+n_1s\beta_1\frac{W}{\eta}-n_1V_{,\xi}+\frac{1}{\eta}\left(\frac{1}{1-2\nu}\right)W_{,\xi}\\
W_{,\xi\xi} &= \left(\frac{\nu}{1-\nu}\right)s\beta_1\left\{-n_1\left(U_{,\eta}+\left(\beta_2+\frac{1}{\eta}\right)U\right)-n_1\frac{V}{\eta}-\left(U_{,\eta\xi}+\left(\beta_2+\frac{1}{\eta}\right)\frac{1}{\eta}U_{,\xi}\right)-\frac{1}{2\nu}\frac{V_{,\xi}}{\eta}\right\}\\
&\quad +\frac{1-2\nu}{2(1-\nu)}s^2\beta_1^2\left[W_{,\eta\eta}+\left(\frac{1}{\eta}+2\beta_2\right)W_{,\eta}+\left(\beta_3+\frac{\beta_2}{\eta}\right)W\right]-n_1W_{,\xi}+\frac{1+\nu}{1-\nu}[(n_1+n_2)\overline{\mathcal{T}}+\overline{\mathcal{T}}_{,\xi}]
\end{aligned}
\tag{22}
$$

where

$$
\beta_1 = e^{n_5\left(\frac{r-b}{a-b}\right)^2},\quad \beta_2=\frac{2n_5(r-b)}{(a-b)^2},\quad \beta_3=\frac{2n_5}{(a-b)^2}+\frac{4n_5^2(r-b)^2}{(a-b)^4} \tag{23}
$$

3. The thermomechanical boundary conditions

It is assumed that the heat transfer is accomplished in a steady-state manner, as expressed in Eq. (15). Therefore, denoting temperatures of the bottom and top surfaces of the plate by $\mathcal{T}_1$ and $\mathcal{T}_2$, respectively (Fig. 1), the general traction and thermal boundary conditions become:

$$
\begin{aligned}
&z=0: \quad \sigma_z=\mathcal{S}(r,\theta),\quad \tau_{z\theta}=0,\quad \tau_{rz}=0,\quad \mathcal{T}(r,0)=\mathcal{T}_1\\
&z=h: \quad \sigma_z=-\mathcal{P}(r,\theta),\quad \tau_{z\theta}=\mathcal{Q}(r,\theta),\quad \tau_{rz}=0,\\
&\qquad \mathcal{T}(r,h)=\mathcal{T}_2 \text{ or } \mathcal{Q}^*=-\kappa\mathcal{T}_{,z}
\end{aligned}
\tag{24}
$$

The following mechanical boundary conditions are considered here for the circular ($b = 0$) and annular plates, without loss of generality:

(i) Circular plate:

Clamped edge (denoted by C):

$$
u(a,\theta,z)=0,\quad v(a,\theta,z)=0,\quad w(a,\theta,z)=0 \tag{25}
$$

Regularity condition at the center:

$$
u(0,\theta,z)=0,\quad v(0,\theta,z)=0,\quad w_{,r}(0,\theta,z)=0 \tag{26}
$$

(ii) Annular plate

Clamped-clamped (C-C) boundary condition:

$$
\begin{aligned}
&u(b,\theta,z)=0,\quad v(b,\theta,z)=0,\quad w(b,\theta,z)=0,\\
&u(a,\theta,z)=0,\quad v(a,\theta,z)=0,\quad w(a,\theta,z)=0
\end{aligned}
\tag{27}
$$

Clamped-movable simply supported (C-S) plate:

$$
\begin{aligned}
&u(b,\theta,z)=0,\quad v(b,\theta,z)=0,\quad w(b,\theta,z)=0,\\
&\sigma_r(a,\theta,z)=0,\quad v(a,\theta,z)=0,\quad w(a,\theta,z)=0
\end{aligned}
\tag{28}
$$

4. The solution procedure

While the temperature distribution may be determined analytically, the displacement field is determined based on Eq. (14) and a combination of the state space and the differential quadrature method. The state space method is employed in the z-direction of the circular plate whereas the differential quadrature rule is used in the radial direction to establish a linear eigenvalue system from which the displacements and stresses can be obtained.

4.1. The analytical thermal solution

Integrating Eq. (15) twice with respect to the transverse coordinate and using Eqs. (3) and (5), yields the analytical distribution of the temperature as:

$$
\begin{aligned}
\mathcal{T}(r,z) &= \frac{\mathcal{T}_2-\mathcal{T}_1}{\int_0^{h(r)}\kappa^{-1}(z)dz}\int_0^z\kappa^{-1}(z)dz+\mathcal{T}_1\\
&= (\mathcal{T}_2-\mathcal{T}_1)\frac{1-e^{-\left[\frac{n_3 z}{h_0 e^{n_5\left(\frac{r-b}{a-b}\right)^2}}\right]}}{e^{n_3}-1}e^{n_3}+\mathcal{T}_1
\end{aligned}
\tag{29}
$$

When the heat flux is specified, e.g.,

$$
\mathcal{Q}^*=\widehat{\mathcal{Q}}^*,\quad \mathcal{T}(r,h)=\mathcal{T}_2 \tag{30}
$$

One has:

$$
\mathcal{T}(r,z)=\widehat{\mathcal{Q}}^*\frac{h}{n_3\kappa_0}\left(e^{-n_3}-e^{-n_3\frac{z}{h}}\right)+\mathcal{T}_2 \tag{31}
$$

4.2. The DQ discretization of the thermo-magneto-elasticity equations

According to the DQ method proposed by Shu [38] derivatives of a given function at any discretization point may be approximated by a weighted linear summation of the function values in the whole domain [39,40]. Location of the sampling points may be chosen according to the Chebyshev-Gauss-Lobatto criterion:

$$
r_i=\frac{1}{2}\left[1-\cos\left(\frac{(i-1)\pi}{N-1}\right)\right](a-b)+b\quad i=1,2,3,\ldots,N \tag{32}
$$

After applying the DQ rule to any arbitrary sample point $\eta_i = r_i/a$, the partial derivatives of the unknown displacements U, V, W with respect to η appeared in Eq. (22) can be expressed as:

$$
\begin{aligned}
&U_{,\eta}|_{\eta=\eta_i}=\sum_{j=1}^N A_{ij}U_j \qquad V_{,\eta}|_{\eta=\eta_i}=\sum_{j=1}^N A_{ij}V_j \qquad W_{,\eta}|_{\eta=\eta_i}=\sum_{j=1}^N A_{ij}W_j\\
&U_{,\eta\eta}|_{\eta=\eta_i}=\sum_{j=1}^N A_{ij}^{(2)}U_j \qquad V_{,\eta\eta}|_{\eta=\eta_i}=\sum_{j=1}^N A_{ij}^{(2)}V_j \qquad W_{,\eta\eta}|_{\eta=\eta_i}=\sum_{j=1}^N A_{ij}^{(2)}W_j\\
&U_{,\eta\xi}|_{\eta=\eta_i}=\sum_{j=1}^N A_{ij}(U_{,\xi})_j \qquad V_{,\eta\xi}|_{\eta=\eta_i}=\sum_{j=1}^N A_{ij}(V_{,\xi})_j \qquad W_{,\eta\xi}|_{\eta=\eta_i}=\sum_{j=1}^N A_{ij}(W_{,\xi})_j
\end{aligned}
\tag{33}
$$

The discretized form of Eq. (24) can be written at the lower surface ($\xi = 0$) as

$$\begin{cases} (U_{,\xi})_i + s\beta_{1i}\left(\sum_{j=1}^{N} A_{ij}W_j + \beta_{2i}W_i\right) = 0 \\ (V_{,\xi})_i - s\dfrac{\beta_{1i}\cot\theta}{\eta_i}W_i = 0 \\ (W_{,\xi})_i + \dfrac{s\nu}{1-\nu}\beta_{1i}\left[\sum_{j=1}^{N} A_{ij}U_j + \left(\beta_{2i} + \dfrac{1}{\eta_i}\right)U_i + \dfrac{\tan\theta}{\eta_i}V_i\right] - \left(\dfrac{1+\nu}{1-\nu}\right)\dfrac{\alpha|_{\xi=0}}{\alpha_1}\overline{T}_i|_{\xi=0} = \Omega \\ \tau_m = s\mu_b\beta_{1i}\left[\sum_{j=1}^{N} A_{ij}U_j + \left(\beta_{2i} + \dfrac{1}{\eta_i}\right)U_i\right] \qquad (i = 1, 2, 3, \ldots, N) \\ L_f = \mu_b s^2\beta_{1i}^2\left[\sum_{j=1}^{N} A_{ij}^{(2)}U_j + \left(2\beta_{2i} + \dfrac{1}{\eta_i}\right)\sum_{j=1}^{N} A_{ij}U_j + \left(\dfrac{\beta_{2i}}{\eta_i} + \beta_{3i} - \dfrac{1}{\eta_i^2}\right)U_i\right] \\ h_z^* = -s\beta_{1i}\left[\sum_{j=1}^{N} A_{ij}U_j + \left(\beta_{2i} + \dfrac{1}{\eta_i}\right)U_i\right] \\ \overline{T}_i = \overline{T}_1 \end{cases} \tag{34}$$

where L_f is the dimensionless Lorentz force and

$$\begin{aligned} \Omega &= \left[1 + \frac{\beta_{6i}}{\beta_{4i}+\beta_{8i}}\left(\frac{1}{a\eta_i}\right)^2(2\tan^2\theta + 1)\right]\overline{\mathcal{S}}_i - \frac{1}{(\beta_{4i}+\beta_{8i})a^2}\left\{\beta_{6i}\sum_{j=1}^{N} A_{ij}^{(2)}\overline{\mathcal{S}}_j + \left[\frac{\beta_{6i}}{\eta_i^2} + \beta_{7i}(\beta_{4i}+\beta_{8i}) - \beta_{6i}(\beta_{5i}+\beta_{9i})\right]\sum_{j=1}^{N} A_{ij}\overline{\mathcal{S}}_j\right\} \\ &= \left(\frac{\beta_{1i}\beta_{4i}\beta_{8i}}{\beta_{4i}+\beta_{8i}}\right)h_0\Gamma W_i - \frac{h_0\Gamma}{(a\eta_i)^2}\left(\frac{\beta_{6i}\beta_{8i}}{\beta_{4i}+\beta_{8i}}\right)\left(\beta_{1i}\sum_{j=1}^{N} A_{ij}W_j + \beta_{2i}W_i\right) - \frac{h_0\Gamma}{a^2} \\ &\quad \times\left(\frac{(\beta_{7i}\beta_{8i} + \beta_{6i}\beta_{9i})(\beta_{4i}+\beta_{8i}) - (\beta_{6i}+\beta_{8i})(\beta_{5i}+\beta_{9i})}{(\beta_{4i}+\beta_{8i})^2}\right)\left(\beta_{1i}\sum_{j=1}^{N} A_{ij}W_j + \beta_{2i}W_i\right) - \frac{h_0\Gamma}{a^2} \\ &\quad \times\left(\frac{\beta_{6i}\beta_{8i}}{\beta_{4i}+\beta_{8i}}\right)\left\{\left(\beta_{1i}\sum_{j=1}^{N} A_{ij}^{(2)}W_j + 2\beta_{2i}\sum_{j=1}^{N} A_{ij}W_j + \beta_{3i}W_i\right) - \frac{\beta_{1i}}{\eta_i^2}[2 + \cos\theta(\tan^2\theta + 1)]W_i\right\} \end{aligned} \tag{35}$$

and

$$\begin{aligned} &\beta_{4i} = k_{l0}e^{f_1(\eta_i)}, \quad \beta_{5i} = \beta_{4i}f_1, \quad \beta_{6i} = T_0\exp[f_2(\eta_i)], \quad \beta_{7i} = \beta_{6i}f_2, \\ &\beta_{8i} = k_{u0}e^{f_3(\eta_i)}, \quad \beta_{9i} = \beta_{8i}f_3, \quad \overline{\mathcal{S}} = \mathcal{S}\Gamma, \quad \Gamma = (1+\nu)(1-2\nu)/\nu E_0 \end{aligned} \tag{36}$$

while on the top surface of the plate ($\xi = 1$), the discretized form of the boundary conditions are:

$$\begin{cases} (U_{,\xi})_i + s\beta_{1i}\left(\sum_{j=1}^{N} A_{ij}W_j + \beta_{2i}W_i\right) = 0 \\ (V_{,\xi})_i - s\dfrac{\beta_{1i}\cot\theta}{\eta_i}W_i = \dfrac{-2(1+\nu)\mathcal{Q}_i}{\exp(n_1)} \\ (W_{,\xi})_i + \dfrac{s\nu}{(1-\nu)}\beta_{1i}\left(\sum_{j=1}^{N} A_{ij}U_j + \left(\beta_{2i} + \dfrac{1}{\eta_i}\right)U_i + \dfrac{\tan\theta}{\eta_i}V_i\right) - \left(\dfrac{1+\nu}{1-\nu}\right)\dfrac{\alpha|_{\xi=1}}{\alpha_1}\overline{T}_i|_{\xi=1} = \dfrac{-(1+\nu)(1-2\nu)\mathcal{P}_i}{(1-\nu)\exp(n_1)} \\ \tau_m = s\mu_b\beta_{1i}\exp(n_4)\left[\sum_{j=1}^{N} A_{ij}U_{ij} + \left(\beta_{2i} + \dfrac{1}{\eta_i}\right)U_i\right] \qquad (i = 1, 2, 3, \ldots, N) \\ L_f = \mu_b s^2\beta_{1i}^2\exp(n_4)\left[\sum_{j=1}^{N} A_{ij}^{(2)}U_j + \left(2\beta_{2i} + \dfrac{1}{\eta_i}\right)\sum_{j=1}^{N} A_{ij}U_j + \left(\dfrac{\beta_{2i}}{\eta_i} + \beta_{3i} - \dfrac{1}{\eta_i^2}\right)U_i\right] \\ h_z^* = -s\beta_{1i}\left[\sum_{j=1}^{N} A_{ij}U_{ij} + \left(\beta_{2i} + \dfrac{1}{\eta_i}\right)U_i\right] \\ \overline{T}_i = \overline{T}_2 \text{ or } \overline{\mathcal{Q}}^* = \overline{T}_{,\xi} \end{cases} \tag{37}$$

where $\overline{\mathcal{Q}}^* = qh\alpha_1/\kappa$ is the dimensionless heat flux.

The discretized form of the edge and regularity conditions (25) and (26) are, respectively:

$$\eta = 1: \quad U_N, V_N, W_N = 0 \tag{38}$$

Regularity condition:

$$\eta = 0: \quad U_1, V_1 = 0, \quad W_N = -\sum_{j=2}^{N} \frac{A_{1j}}{(\beta_{21} + A_{11})} W_j \tag{39}$$

The discretized form of Eqs. (27) and (28) are, respectively:

$$\begin{array}{l} \eta = 0: \quad U_1, V_1, W_1 = 0, \\ \eta = 1: \quad U_N, V_N, W_N = 0 \end{array} \tag{40}$$

and

$$\begin{array}{l} \eta = 0: \quad U_1, V_1, W_1 = 0, \\ \eta = 1: \quad \sigma_{\eta N}, V_N, W_N = 0 \end{array} \tag{41}$$

4.3. The state space method

Assemblage of the discretized forms of the three governing equations appeared in Eq. (22) for the ith sampling point, leads to the following matrix form of the state space equation

$$\Xi_{i,\xi}(\xi) = \mathcal{D}_i \Xi_i(\xi) + \mathcal{G}_i \Theta_i(\xi) \tag{42}$$

where

$$\begin{aligned} \Xi_i^T(\xi) &= \left[\mathbf{U}_i \quad \mathbf{V}_i \quad \mathbf{W}_i \quad \mathbf{U}_{i,\xi} \quad \mathbf{V}_{i,\xi} \quad \mathbf{W}_{i,\xi} \right], \quad \Theta_i^T(\xi) \\ &= \left[\overline{T}_{1i} \quad 0 \quad 0 \quad 0 \quad 0 \quad \overline{T}_{,\xi i} \right] \end{aligned} \tag{43}$$

Ξ_i is the global state vector at an arbitrary layer (ξ) of the plate and $\mathcal{D}_i$ is the coefficient matrix evaluated at the ith sampling point. Elements of the $\mathcal{D}_i$ and $\mathcal{G}_i$ matrices are given in Appendix.

By considering all edge conditions, Eq. (42) can be rewritten as follows

$$\widehat{\Xi}_{i,\xi}(\xi) = \widehat{\mathcal{D}}_i \widehat{\Xi}_i(\xi) + \widehat{\mathcal{G}}_i \widehat{\Theta}_i(\xi) \tag{44}$$

where the hat symbol denotes the modified matrices resulting after incorporation of the edge conditions. The boundary conditions may be incorporated through assembling of the boundary conditions and the governing equations into an augmented system of equations.

According to the algebra rules, the general solution to Eq. (44) is:

$$\widehat{\Xi}_i(\xi) = e^{\xi \widehat{\mathcal{D}}_i} \widehat{\Xi}_i(0) + \widehat{\mathcal{H}}_\xi \tag{45}$$

where the $\widehat{\mathcal{H}}_\xi$ is the thermal loading vector

$$\widehat{\mathcal{H}}_\xi = \int_0^\xi e^{(\xi-\tau)\widehat{\mathcal{D}}} \widehat{\Theta}(\tau) t(\tau) d\tau \tag{46}$$

The relevant integration is implemented via the numerical quadrature technique in the present study. Eq. (45) establishes the global transfer relation from the state vector on the bottom surface ($\widehat{\Xi}_i(0)$) to that at an arbitrary layer ξ of the plate through $\exp(\xi \widehat{\mathcal{D}}_i)$. Setting $\xi = 1$ in Eq. (45) gives

$$\widehat{\Xi}_i(1) = e^{\widehat{\mathcal{D}}_i} \widehat{\Xi}_i(0) + \widehat{\mathcal{H}}_1 \tag{47}$$

where $\exp(\widehat{\mathcal{D}}_i)$ is the global transfer matrix and $\widehat{\mathcal{H}}_1$ is obtained by setting the upper limit of the integral appeared in Eq. (46) to unity. $\widehat{\Xi}_i(1)$ and $\widehat{\Xi}_i(0)$ are the values of the state variables at the upper and lower surfaces of the plate, respectively.

By substituting the boundary conditions presented in Eqs. (34)–(41) and Eq. (42) into Eq. (47), the following algebraic system of equations is obtained

$$\mathcal{M}\mathbf{X} = \mathcal{R} \tag{48}$$

where $\mathcal{M}$ is a $6(N-2) \times 6(N-2)$ matrix, $\mathcal{R}$ is the external thermo-magneto-mechanical load vector and

$$\begin{aligned} \mathbf{X}^T = [\, &\mathbf{U}_i(0) \quad \mathbf{V}_i(0) \quad \mathbf{W}_i(0) \quad \mathbf{U}_i(1) \quad \mathbf{V}_i(1) \quad \mathbf{W}_i(1) \,], \quad (i \\ &= 2, 3, \ldots, N-1) \end{aligned} \tag{49}$$

By solving Eq. (48), all of the state variables are obtained at $\xi = 0$ and $\xi = 1$. Thereafter, Eqs. (42) and (13) may be used to determine the displacement and stress components of the functionally graded annular/circular plate.

5. Results and discussions

5.1. General specifications employed for the parametric studies

Section 5 contains verification as well as new examples. In presenting the parametric study and derivation of the main results of the paper, it is assumed that the plate is a variable thickness Aluminum/Alumina (top layer is fabricated from Alumina) transversely graded one. Material properties of the constituent materials are given in Table 1. According to Eqs. (1)–(4), the material properties vary exponentially in the thickness direction of the plate. Since the thickness vary in the radial direction, gradients of variations of the material properties are higher in thinner sections.

Geometric and loading parameters of the plate and specifications of the elastic foundation are:

$a = 1$ m, $b = 0.01$ m, $s = 0.02$, $n_5 = 0.1$, $f_1, f_2, f_3 = 0.2$,
$k_{l0} = k_{u0} = 0.2$ GN/m^3,
$T = 0.2$ GN/m, $\mathcal{P}_0 = \mathcal{Q}_0 = 1$ GPa, $\mathcal{A}_1, \mathcal{A}_2, \mathcal{B}_1, \mathcal{B}_2 = 0.1$,
$\mu_0 = 4\pi \times 10^{-7}$ H/m

Unless otherwise stated, the traction and thermal boundary conditions of the plate are:

$\mathcal{T}_1 = 100$ C, $\mathcal{T}_2 = 500$ C, $\sigma_z|_{\xi=1} = -\mathcal{P}$, $\tau_{\theta z}|_{\xi=1} = \mathcal{Q}$

5.2. Convergence analysis

Number of the radial sampling points may significantly affect accuracy of the results. The accomplished convergence analysis showed that the displacement parameters are more

Table 1 – Mechanical and thermal properties of the constituent materials of the considered annular FG plates [32].

Material	E (GPa)	ν	α (C^{-1})	κ (W/mK)
Aluminum	70	0.33	23.1e−6	237
Alumina	116	0.33	8.7e−6	1.78

convergent that the magnetic stresses; because the magnetic stresses (as other stress components) are themselves dependent on not only the displacement components but also on their radial derivatives. For this reason, results of the convergence analysis of the dimensionless Maxwell's electromagnetic stress and the lateral deflection are reported here. In this regard, a functionally graded variable thickness clamped annular plate with the specifications mentioned in Section 5.1 is adopted and results of a representative point located at $\eta^* = \frac{r-b}{a-b} = 0.5$, $\xi = 0$, and $\theta = \pi/4$ are adopted ($H_z = 3 \times 10^8$ A/m). The results obtained for various numbers of the sampling points are reported in Table 2. As results of Table 2 imply, a number of sampling points equals $N = 11$ guarantees the convergence. For this reason, this number has been used in the next analyses.

5.3. *Verification of the results*

As a verification example, results of a clamped functionally graded circular plate with uniform thickness subjected to an asymmetric distributed transverse load considered previously by Nie and Zhong [41] are reexamined. Geometric and material specifications of the plate are:

$$h/a = 0.1, \quad E_0 = 380 \text{ GPa}, \quad \nu = 0.3, \quad n_1 = 1, \quad \mathcal{P} = 1 \text{ GPa}$$

Present results for the transverse shear stress $\tau_{\theta\xi}$ are compared with those reported by Nie and Zhong [41] in Table 3, for various points of thickness of a section located at $\eta^* = 0.5$, $\theta = \pi/4$. As may be seen from results of Table 3, there is an excellent agreement between present results and results of Nie and Zhong.

5.4. *Influence of various parameters on the elastic behavior of the FGM annular plate*

Results of the following thermal conditions are used in behavior study of the plate:

(i) Dirichlet-type thermal boundary condition:

$$\mathcal{T}_1 = 100 \text{ C}, \quad \mathcal{T}_2 = 500 \text{ C} \tag{50}$$

(ii) Dirichlet-Neumann thermal boundary condition:

$$\mathcal{Q}^* = 100 \text{ W/mC}, \quad \mathcal{T}_2 = 500 \text{ C} \tag{51}$$

In the present section, the magnetic intensity is adopted as $H_z = 2.23 \times 10^9$ A/m and unless otherwise stated, n_1, n_2, n_3 and n_4 may be determined based on:

$$n_1 = \ln\left(\mathrm{E}|_{\xi=1}/\mathrm{E}|_{\xi=0}\right), \quad n_2 = \ln\left(\alpha|_{\xi=1}/\alpha|_{\xi=0}\right), \quad n_3 = \ln\left(\kappa|_{\xi=1}/\kappa|_{\xi=0}\right), \quad n_4 = \ln\left(\mu_0|_{\xi=1}/\mu_0|_{\xi=0}\right) \tag{52}$$

As a first stage in the parametric study, influence of the heterogeneity exponents on the resulting displacement and stress components is evaluated. In this regard, three values are chosen for these exponents: $n_1 = n_2 = n_3 = n_4 = 0.25, 0.5, 0.75$ and the resulting transverse displacement and stress distributions are plotted in Fig. 2, for a section located at the middle radius of the plate ($\theta = \pi/4$). According to Fig. 2a–c, since increasing the heterogeneity exponents increases rigidity as well as thermal expansion and thermal conductivity of the plate, the section tends to move outwards in higher exponents of the clamped-clamped plate. Therefore, the inflection point of the deformed plate moves toward the outer edge of the plate; so that direction of both radial and transverse displacements of the plate change. The changes in the transverse distributions of the in-plane stresses, i.e., the radial and circumferential stresses confirm the shift in the location of the inflection section, too. Since the stiffer material exhibits greater resistance against deformation, the simultaneous increase in the thermal expansion has led to higher in-plane and transverse stresses. As Fig. 2h and i shows, since the top surface of the plate is prone to a circumferential shear stress, the in-plane and transverse shear stresses of the top surface are no-zero quantities. As may be noted, due to presence of the shear traction, locations of the maximum stress of the two components of the transverse shear stresses are not coincident.

Effects of the transverse temperature gradient are illustrated in Fig. 3, for $\Delta\mathcal{T} = 400, 500, 600$ retaining temperature of the bottom layer at $\mathcal{T}_1 = 50$C. It's worth mentioning that due to the thickness variability, the temperature gradient is higher in narrower sections of the plate. As may be expected, all of the

Table 2 – Results of the convergence analysis in terms of the dimensionless transverse deflection W and dimensionless Maxwell's electromagnetic stress τ_m against the number of the grid points, for a point located at $\eta^* = 0.5$, $\xi = 0$, $\theta = \pi/4$ of the clamped annular plate ($H_z = 3 \times 10^8$ A/m).

Quantity	N								
	3	5	7	9	11	13	15	17	19
W	1.5260	1.7523	1.7660	1.9567	1.9568	1.9567	1.9567	1.9568	1.9569
τ_m	−0.2374	−0.1545	−0.1531	−0.1635	−0.1636	−0.1635	−0.1635	−0.1636	−0.1637

Table 3 – A comparison between present transverse shear stress ($\tau_{\theta\xi}$) results and those of Nie and Zhong [41] for a uniform thickness FG circular plate under an asymmetric transverse load.

Source	ξ									
	0.0	0.1	0.2	0.3	0.5	0.6	0.7	0.8	0.9	1.0
Nie and Zhong [41]	0.000	0.302	0.565	0.771	1.033	1.062	1.023	0.812	0.471	0.000
Present	0.000	0.301	0.5649	0.770	1.033	1.062	1.023	0.812	0.471	0.000

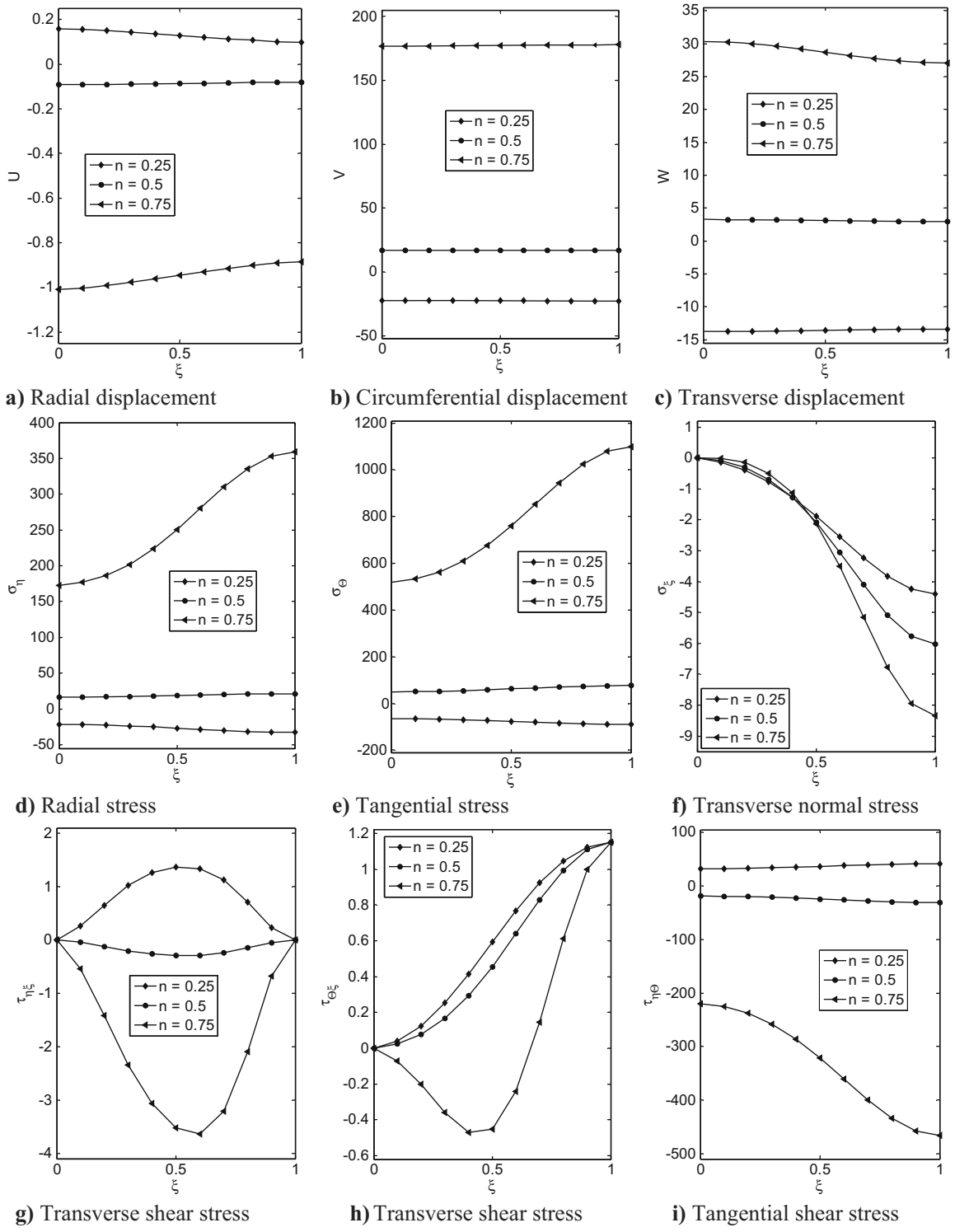

Fig. 2 – Effects of the heterogeneity exponents on the resulting transverse distributions of the displacement and stress components of the clamped annular plate at ($\eta^* = 0.5$, $\theta = \pi/4$).

displacement and stress components have increased by increasing the transverse temperature difference. However, in contrast to the material properties that exponentially affect the results, present results are almost proportional to magnitude of the difference between temperatures of the top and bottom layers. However, effects of rates of variations of the temperature in the radial and transverse directions cannot be ignored.

As the next stage, influence of coefficients of the elastic foundation on the elastic responses is investigated. It is evident that as the elastic foundation becomes stiffer, it absorbs much strain energy and consequently, the resulting

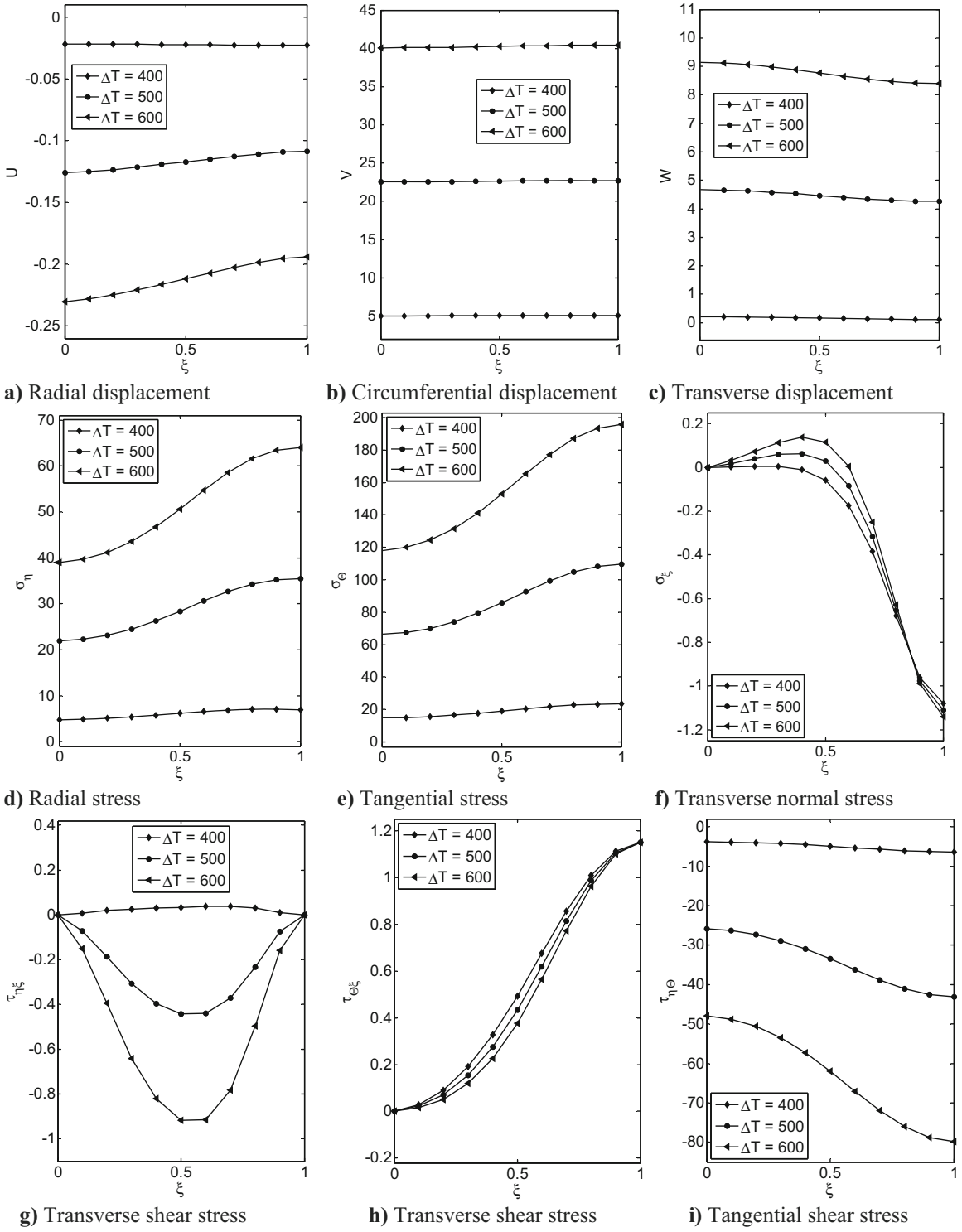

Fig. 3 – Effects of temperature of the top surface of the clamped annular plate on transverse distributions of the displacement and stress components at ($\eta^* = 0.5$, $\theta = \pi/4$) ($\mathcal{T}_1 = 50C$).

displacement and stresses become smaller, as Fig. 4 shows. Results of Fig. 4 are depicted for a section located at ($\eta^* = 0.5$, $\theta = \pi/6$), for $n_4 = 0.1$, k_{l0}, k_{u0}, $T_0 = k = 10$, 20, 30. In this case wherein the plate is squeezed from the top and bottom layers and radial movement is restricted at the edges, the stress field resembles a hydrostatic one; so that the normal stresses are compressive/tensile ones for all points of the plate. For this reason, magnitudes of the transverse stresses are negligible. Furthermore, due to the elastic foundation reaction, the in-plane shear stress of the lower surface of the plate is larger than the previous cases.

Effects of the magnitude of the intensity of the magnetic field on the elastic responses of the clamped annular plate are studied in Fig. 5, for k_{l0}, $k_{u0} = 10$ GN/m^3, $T_0 = 10$ N/m and $H_z =$

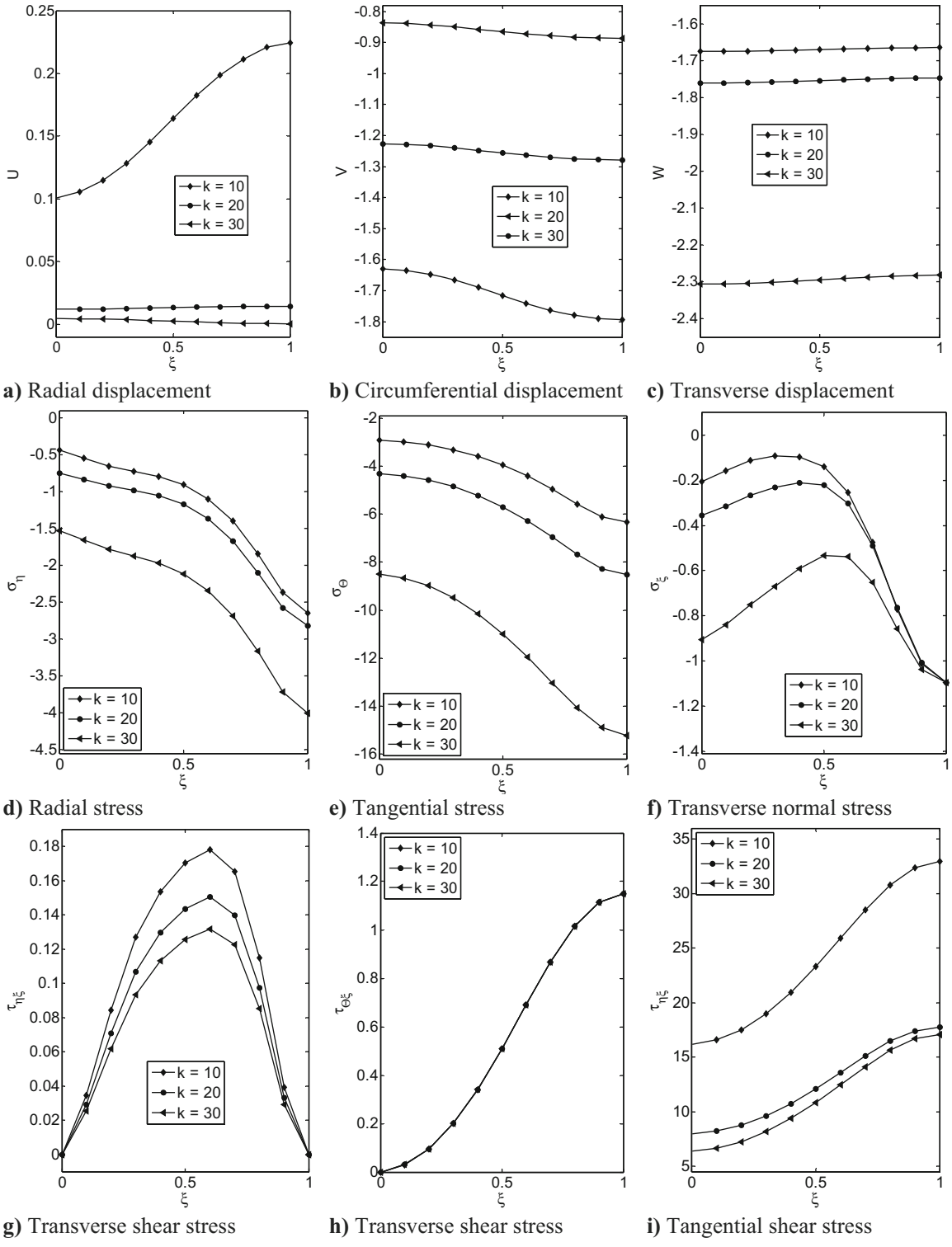

Fig. 4 – Effects of the coefficient of the elastic foundation on transverse distributions of the displacements and stresses of the clamped-clamped annular plate at ($\eta^* = 0.5$, $\theta = \pi/6$).

$(0.5, 1, 1.5, 2) \times 10^9$ A/m at a section located at ($\eta^* = 0.5$, $\theta = \pi/4$). Results of Fig. 5 imply that the magnetic field increases the stiffness of the plate and consequently, reduces the displacements and stresses of the plate; so that the resulting displacement and in-plane curves are almost parallel. However, the distances between the successive curves reduce by increasing the magnetic intensity, so that finally, they tend to an asymptotic (saturated) response. However, results of Fig. 5 are affected by other factors such as the temperature gradient, as well. Fig. 5a, c, d and f reveals that although rotation of the section is negligible in this case, deformation of the thickness and gradients of the in-plane stresses are noticeable.

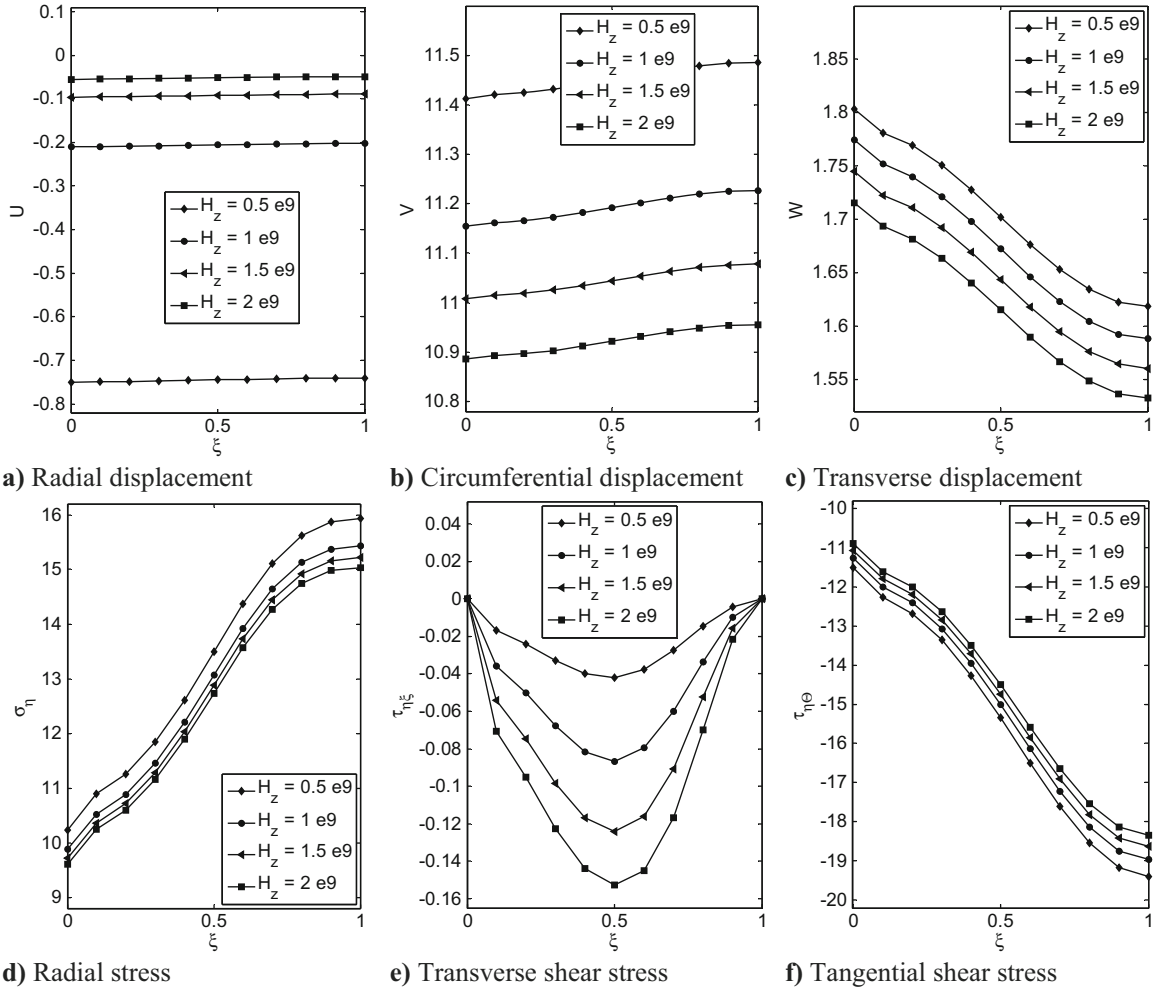

Fig. 5 – Influence of the intensity of the magnetic field on transverse distributions of the displacements and stresses of the clamped-clamped annular plate at ($\eta^* = 0.5$, $\theta = \pi/4$).

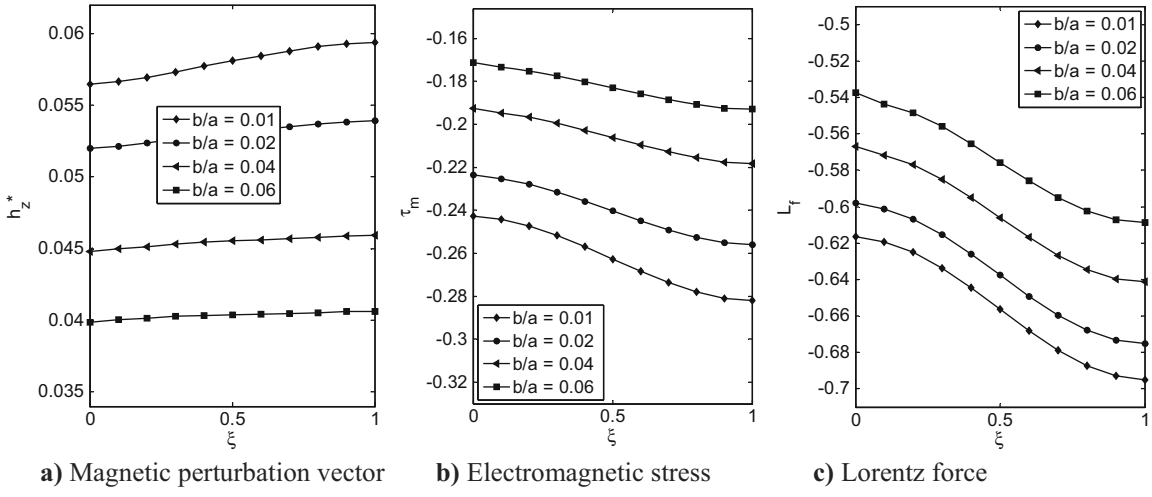

Fig. 6 – Effect of the radius ratio on transverse distributions of the induced electromagnetic forces and stresses of the clamped-clamped annular plate at ($\eta^* = 0.5$, $\theta = \pi/4$).

5.5. *Influence of various parameters on the induced magnetic forces and stresses*

As may be deduced from Eqs. (19), (20) and (22), the magnetic forces and stresses affect the elastic quantities and vice versa. Effects of the magnetic quantities on the elastic responses are studied in the previous section and present section is devoted to study influences of various parameters on the magnetic stresses and body (Lorentz) forces. Unless otherwise stated, n_1, n_2, n_3, n_4 correspond to Eq. (52) and $H_z = 3 \times 10^8$ A/m.

Effects of the radius ratio on the dimensionless magnetic perturbation vector, electromagnetic stress, and Lorentz force are demonstrated in Fig. 6. In this regard, the transverse distributions of the mentioned quantities are studied for a section located at ($\eta^* = 0.5$, $\theta = \pi/4$) of a clamped-clamped annular plate ($n_4 = 0.1$). Results of Fig. 6 show that as the inner radius increases, movability of the plate reduces and according to Eqs. (19) and (20), less magnetic quantities are induced in the plate. However, since deformation of the top layer is greater, larger Lorentz force and electromagnetic stress are induced there.

Table 4 – Influence of the plate thickness on the magnitudes of the induced dimensionless magnetic quantities, at (η^*, $\xi = 0.5$, $\theta = \pi/3$) of a clamped-simply supported annular plate.

Induced magnetic quantity	h_0/a		
	0.05	0.1	0.15
$\lvert h_z^* \rvert$	0.0001	0.0002	0.0003
$\lvert \tau_m \rvert$	0.0005	0.001	0.0011
$\lvert L_f \rvert$	0.0123	0.0467	0.0638

Influence of the thickness ratio on the induced magnetic quantities may be observed in results of Table 4 that are reported for a point located at (η, $\xi = 0.5$, $\theta = \pi/3$) of a clamped-simply supported annular plate (for diversity). These results show that the induced quantities grow non-proportionally by increasing thickness of the plate; so that very huge quantities are induced in the thicker plates.

After checking effects of the geometric ratios, effects of heterogeneity exponents of the elasticity modulus, thermal

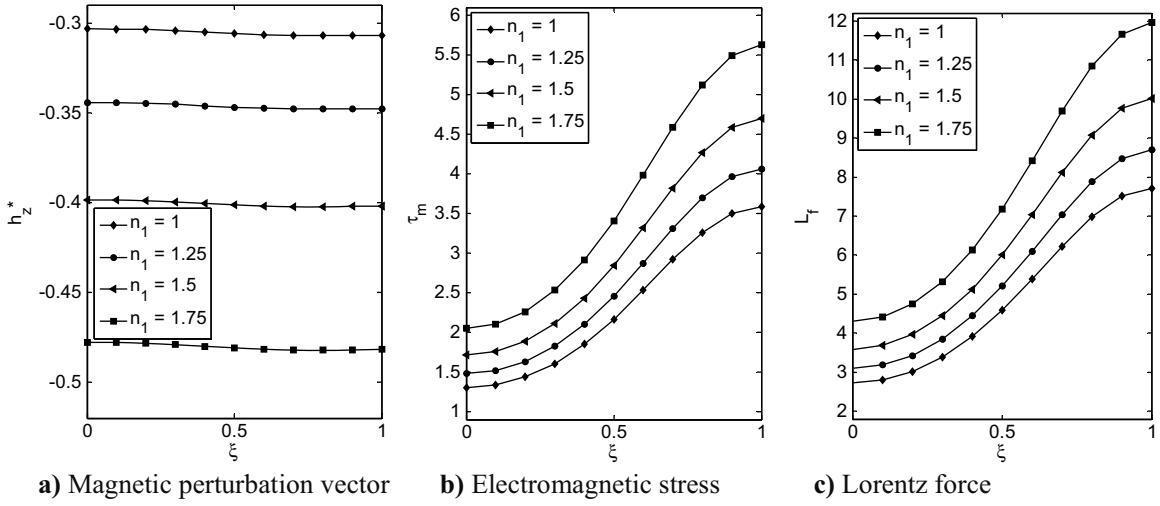

Fig. 7 – Effects of the heterogeneity exponent of the elastic modulus on the transverse distributions of the induced magnetic quantities of the clamped circular plate at ($\eta^* = 0.5$, $\theta = \pi/4$).

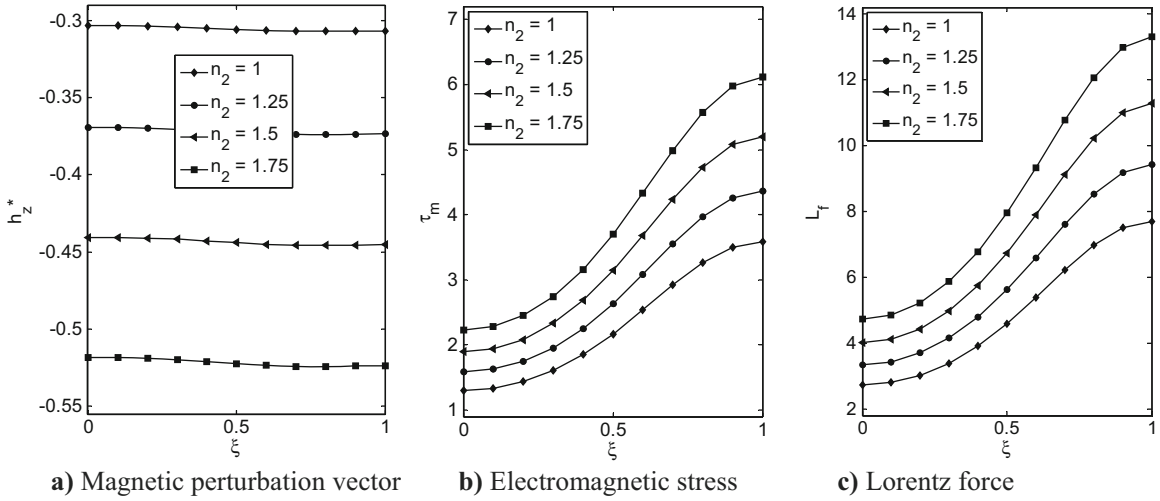

Fig. 8 – Effects of exponent of the thermal expansion coefficient on the transverse distributions of the induced magnetic quantities of the clamped circular plate at ($\eta^* = 0.5$, $\theta = \pi/4$).

expansion, thermal conductivity, and magnetic permeability on the induced magnetic quantities are investigated and the relevant effects on transverse distributions of a section located at ($\eta^* = 0.5$, $\theta = \pi/4$) of the plate are illustrated in Figs. 7–10, respectively. The considered plate is circular and its top surface is subjected to a $\mathcal{Q}^* = 100$ W/m^2 heat flux. Results of Figs. 7–9 are extracted for n_1, n_2, $n_3 = 1$, 1.25, 1.75, 2 and $n_4 = 1$ whereas results of Fig. 10 are derived for $n_4 = 0.5$, 0.75, 1, 1.25 and n_1, n_2, $n_3 = 1$.

Results of Fig. 2 has shown that these exponents have significant effects on the resulting displacement components and therefore, it may be inferred that they may have pronounced effects on the induced magnetic quantities. Figs. 7 and 8 imply that exponents of the elasticity modulus and thermal expansion lead to almost similar trends; so that the induced quantities increase, to some extent, proportionally by increasing the exponents but for the special materials considered, sensitivity to magnitude of the thermal expansion exponent is higher. Different trends may be seen in Figs. 9 and 10. Fig. 10 implies that using a graded permeability may affect the induced Lorentz force and electromagnetic stress quantities of the intermediate and top layers only.

Ratio of the shear to normal tractions of the top surface (the load ratio $LR = \mathcal{Q}_0/\mathcal{P}_0$) may considerably affect the resulting deformations and consequently, the induced magnetic quantities. Effects of the load ratio on the transverse distributions of the magnetic quantities at ($\eta = 0.5$, $\theta = \pi/4$) of the mentioned plate may be studied in Fig. 11 for four load ratios ($LR = 2, 4, 6, 8$). Since increased load ratios bring about higher radial displacements at the top layer of the plate, the induced magnetic quantities increase monotonically, at all points of the section, by an increase in the load ratio, as may be noted in Fig. 11.

Since the distribution of the material properties of the plate is asymmetric, even uniform heating of the plate leads to bending of the sections of the plate and consequently, to induction of the magnetic and electromagnetic quantities. In this regard, effects of the heat flux is investigated for four values: $\mathcal{Q}^* = 100, 200, 300, 400$ W/mC and the resulting transverse distributions of the dimensionless induced quantities are depicted in Fig. 12. Trends of these results are in agreement

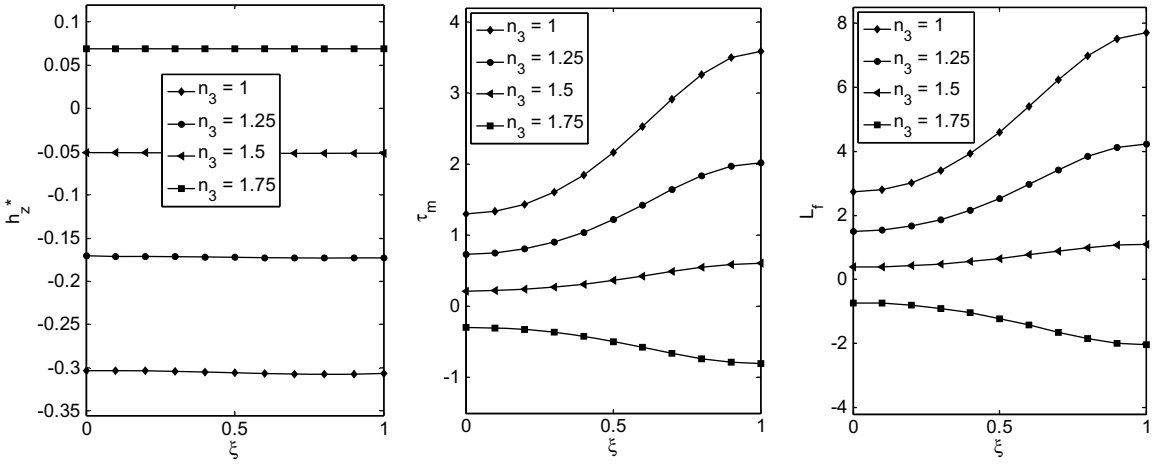

a) Magnetic perturbation vector **b)** Electromagnetic stress **c)** Lorentz force

Fig. 9 – Effects of exponent of the thermal conduction on the transverse distributions of the induced magnetic quantities of the clamped circular plate at ($\eta^* = 0.5$, $\theta = \pi/4$).

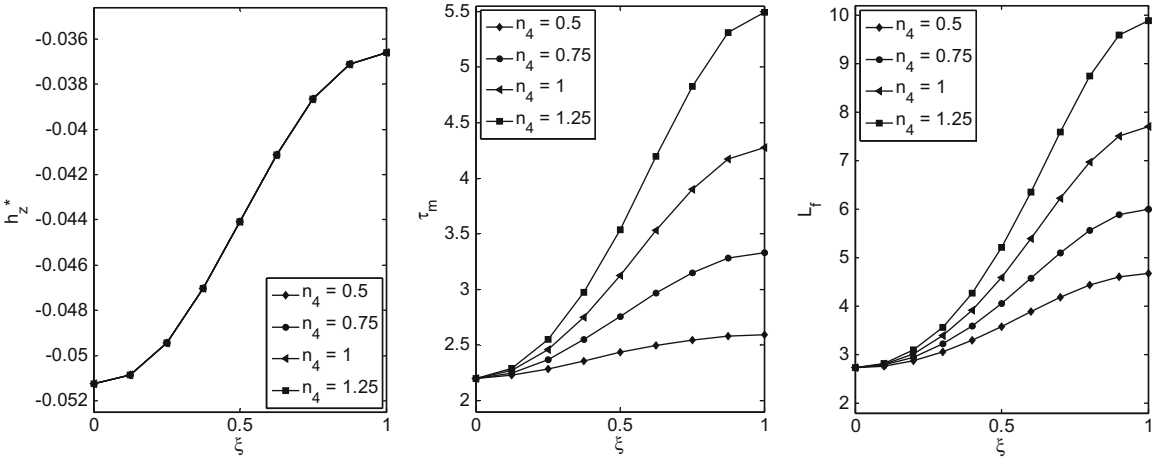

a) Magnetic perturbation vector **b)** Electromagnetic stress **c)** Lorentz force

Fig. 10 – Effects of exponent of the magnetic permeability on the transverse distributions of the induced magnetic quantities of the clamped circular plate at ($\eta^* = 0.5$, $\theta = \pi/4$).

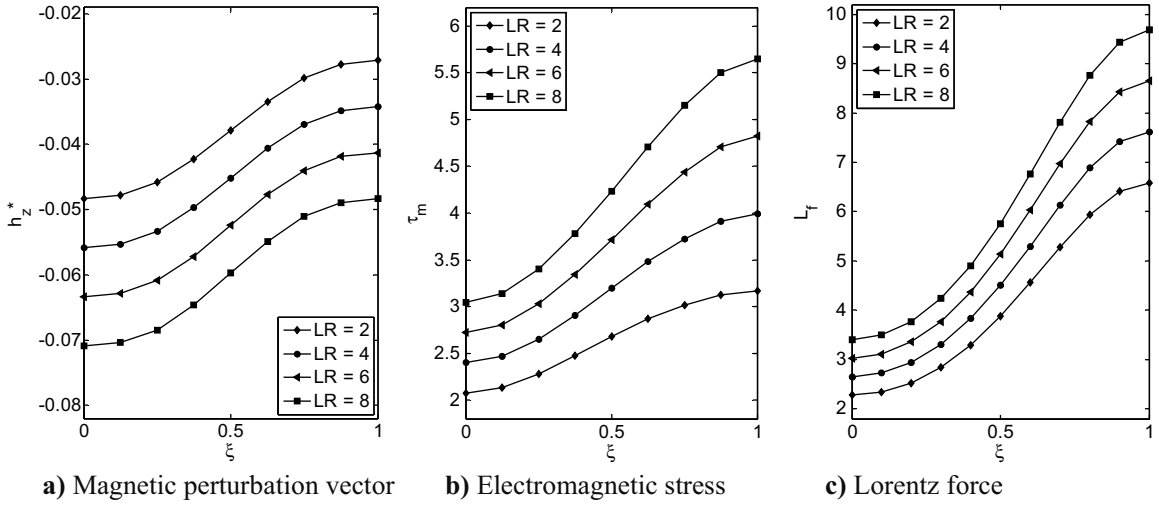

a) Magnetic perturbation vector **b)** Electromagnetic stress **c)** Lorentz force

Fig. 11 – Influence of the loads ratio on the transverse distributions of the induced magnetic quantities of the clamped circular plate at ($\eta^* = 0.5$, $\theta = \pi/4$).

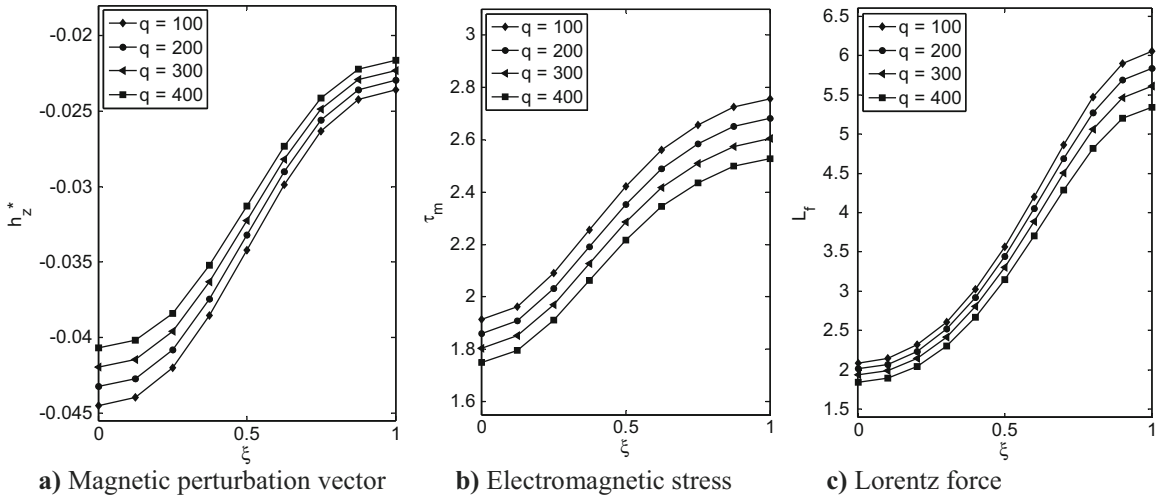

a) Magnetic perturbation vector **b)** Electromagnetic stress **c)** Lorentz force

Fig. 12 – Influence of the conduction heat flux on the transverse distributions of the induced magnetic quantities of the clamped circular plate at ($\eta^* = 0.5$, $\theta = \pi/4$).

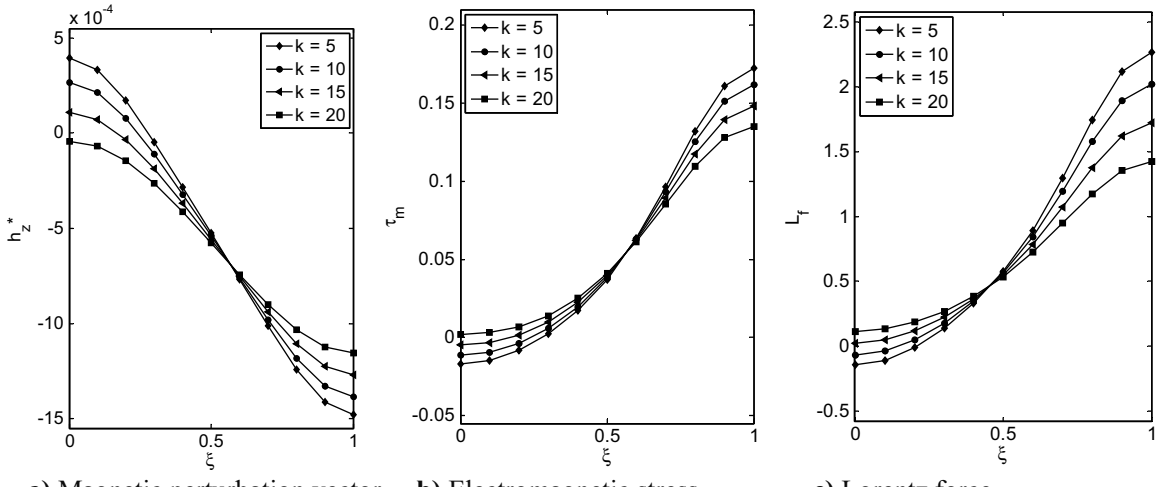

a) Magnetic perturbation vector **b)** Electromagnetic stress **c)** Lorentz force

Fig. 13 – Influence of the foundation stiffness on the transverse distributions of the induced magnetic quantities of the clamped circular plate at ($\eta^* = 0.5$, $\theta = \pi/3$).

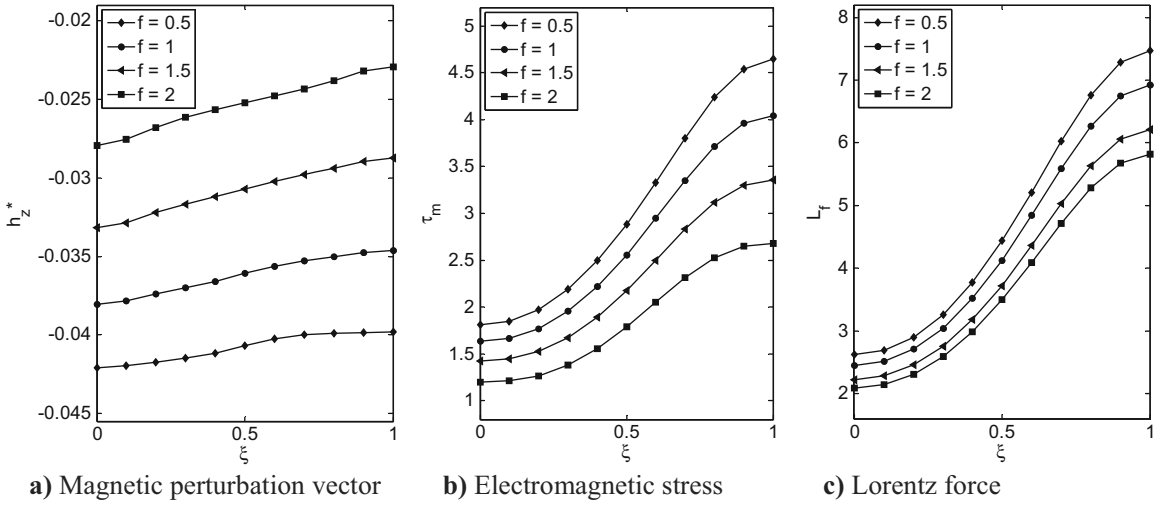

Fig. 14 – Influence of exponent of the stiffness quantities of the elastic foundation on the transverse distributions of the induced magnetic quantities of the clamped circular plate at ($\eta^* = 0.5$, $\theta = \pi/4$).

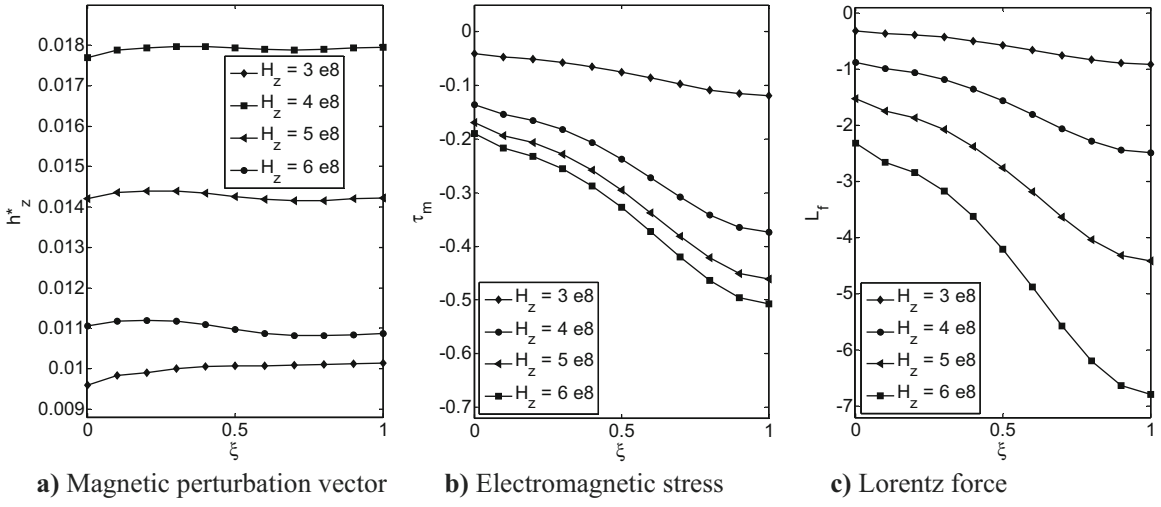

Fig. 15 – Effects of intensity of the magnetic field on the transverse distributions of the induced magnetic quantities of the clamped circular plate at ($\eta^* = 0.5$, $\theta = \pi/4$).

with the suggested conclusions, i.e., the induced magnetic quantities increase with the conduction heat flux.

Compliance of the elastic foundation affects the relative radial displacement of the layers with respect to the neutral layer of the plate and consequently, magnitude of the induced magnetic quantities. Results of Fig. 13 confirm this conclusion. As may be readily seen in Fig. 13, the induced quantities are higher for more compliant elastic foundations whereas the induced magnetic quantities of the neutral plane of the plate have almost remained unchanged. On the other hand, non-uniformity of the elastic foundation may significantly affect the radial and transverse distributions of the displacement components and consequently, transverse distributions of the induced magnetic quantities, as may be seen in Fig. 14.

Finally, effects of intensity of the magnetic field on the transverse distributions of the dimensionless induced magnetic quantities are illustrated in Fig. 15 ($n_4 = 1$). Due to presence of all the mechanical, thermal, and magnetic loads, and especially, interactions of their effects on the plate, results have not changed in regular trends, however, the induced quantities increase by increasing the intensity of the magnetic field.

6. Conclusions

A semi-analytical thermo-magneto-elasticity solution is presented for functionally graded variable thickness annular plates undergoing asymmetric shear and normal tractions and thermal and magnetic fields and resting on non-uniform elastic foundations. Results reveal that:

- Exponents of the elasticity modulus, thermal expansion, and heat conductivity significantly affect location of the inflection section of the plate and consequently, distributions of the displacement and stress components.
- Effects of rates of variations of the temperature in the transverse direction cannot be ignored, especially when the thickness is variable.

- In stiffer foundations, the stress field resembles a hydrostatic field; so that magnitudes of the transverse stresses become negligible but the in-plane shear stress of the lower surface of the plate becomes larger.
- The magnetic actuation increases the stiffness of the plate and consequently, reduces the displacements and stresses of the plate
- Larger magnetic quantities are induced in plates with smaller inner radius, higher material exponents, and larger shear tractions and these quantities grow by increasing thickness of the plate.
- The induced magnetic quantities increase with the conduction heat flux.
- The induced magnetic quantities are higher for more compliant elastic foundations.

Appendix

Elements of the state matrix $\mathcal{D}_i$ of Eq. (42) of the ith discretization point are

$$\mathcal{D}_i=\begin{bmatrix} 0_{N\times N} & 0_{N\times N} & 0_{N\times N} & I_{N\times N} & 0_{N\times N} & 0_{N\times N}\\ 0_{N\times N} & 0_{N\times N} & 0_{N\times N} & 0_{N\times N} & I_{N\times N} & 0_{N\times N}\\ 0_{N\times N} & 0_{N\times N} & 0_{N\times N} & 0_{N\times N} & 0_{N\times N} & I_{N\times N}\\ d^{41}_{N\times N} & d^{42}_{N\times N} & d^{43}_{N\times N} & d^{44}_{N\times N} & 0_{N\times N} & d^{46}_{N\times N}\\ d^{51}_{N\times N} & d^{52}_{N\times N} & d^{53}_{N\times N} & 0_{N\times N} & d^{55}_{N\times N} & d^{56}_{N\times N}\\ d^{61}_{N\times N} & d^{62}_{N\times N} & d^{63}_{N\times N} & d^{64}_{N\times N} & d^{65}_{N\times N} & d^{66}_{N\times N} \end{bmatrix}_{6N\times 6N} \tag{A.1}$$

where I is the identity matrix and ($i, j = 1, 2, \ldots, N$)

$$d^{41}_{ij}=\begin{cases} s^2\beta^2_{1i}\left\{-\left(\frac{2(1-\nu)}{1-2\nu}+\mu_b\right)\left[A^{(2)}_{ii}+\left(\frac{1}{\eta_i}+2\beta_{2i}\right)A_{ii}+\left(\frac{\beta_{2i}}{\eta_i}+\beta_{3i}-\frac{1}{\eta_i^2}\right)+\frac{1}{\eta_i^2}\right]\right\}; & (i=j)\\ -s^2\beta^2_{1i}\left\{\left(\frac{2(1-\nu)}{1-2\nu}\right)\left[\sum_{j=1}^{N}A^{(2)}_{ij}+\left(\frac{1}{\eta_i}+2\beta_{2i}\right)\sum_{j=1}^{N}A_{ii}\right]-\mu_b\left[A^{(2)}_{ii}+\left(\frac{1}{\eta_i}+2\beta_{2i}\right)A_{ii}\right]\right\}; & (i\neq j)\end{cases}$$

$$d^{42}_{ij}=\begin{cases} \frac{s^2\beta^2_{1i}}{\eta_i}\left\{\frac{2(1-\nu)}{(1-2\nu)}\frac{1}{\eta_i}-\frac{2\nu}{1-2\nu}(A_{ii}+\beta_{2i})-\left[A_{ii}+\left(\beta_{2i}-\frac{1}{\eta_i}\right)\right]\right\}; & (i=j)\\ -\left(\frac{1}{1-2\nu}\right)s^2\beta^2_{1i}\frac{1}{\eta_i}\sum_{j=1}^{N}A_{ij}; & (i\neq j)\end{cases}$$

$$d^{43}_{ij}=\begin{cases} -n_1 s\beta_{1i}(A_{ii}+\beta_{2i}); & (i=j)\\ -n_1 s\beta_{1i}\sum_{j=1}^{N}A_{ij}; & (i\neq j)\end{cases},\quad d^{44}_{ij}=\begin{cases} -n_1; & (i=j)\\ 0; & (i\neq j)\end{cases}$$

$$d^{46}_{ij}=\begin{cases} s\beta_{1i}\left\{\frac{2\nu}{(1-2\nu)}\frac{1}{\eta_i}-\left(\frac{2\nu}{1-2\nu}\right)\left[A_{ii}+\left(\beta_{2i}+\frac{1}{\eta_i}\right)\right]-(A_{ii}+\beta_{2i})\right\}; & (i=j)\\ -\left(\frac{1}{1-2\nu}\right)s\beta_{1i}\sum_{j=1}^{N}A_{ij}; & (i\neq j)\end{cases}$$

$$d^{51}_{ij}=\begin{cases} s^2\beta^2_{1i}\left\{\frac{2\nu}{(1-2\nu)\eta_i}(A_{ii}+\beta_{2i})+\frac{2(1-\nu)}{(1-2\nu)\eta_i^2}+\left[\frac{1}{\eta_i}A_{ii}+\left(\frac{\beta_{2i}}{\eta_i}-\frac{1}{\eta_i^2}\right)\right]\right\}; & (i=j)\\ \frac{1}{1-2\nu}s^2\beta^2_{1i}\frac{1}{\eta_i}\sum_{j=1}^{N}A_{ij}; & (i\neq j)\end{cases}$$

$$d^{52}_{ij}=\begin{cases} s^2\beta^2_{1i}\left\{-\left[A^{(2)}_{ii}+\left(2\beta_{2i}+\frac{1}{\eta_i}\right)A_{ii}+\left(\beta_{2i}+\beta_{3i}-\frac{1}{\eta_i^2}\right)\right]+\frac{2(1-\nu)}{(1-2\nu)\eta_i^2}\right\}; & (i=j)\\ -s^2\beta^2_{1i}\left[\sum_{j=1}^{N}A^{(2)}_{ij}+\left(2\beta_{2i}+\frac{1}{\eta_i}\right)\sum_{j=1}^{N}A_{ij}\right]; & (i\neq j)\end{cases} \tag{A.2}$$

$$d^{53}_{ij}=\begin{cases} -\frac{n_1 s\beta_{1i}}{\eta_i}; & (i=j)\\ 0; & (i\neq j)\end{cases},\quad d^{55}_{ij}=\begin{cases} -n_1; & (i=j)\\ 0; & (i\neq j)\end{cases},\quad d^{56}_{ij}=\begin{cases} -\frac{1}{\eta_i(1-2\nu)}; & (i=j)\\ 0; & (i\neq j)\end{cases},$$

$$d^{61}_{ij}=\begin{cases} -n_1\left(\frac{\nu}{1-\nu}\right)s\beta_{1i}\left[A_{ii}+\left(\beta_{2i}+\frac{1}{\eta_i}\right)\right]; & (i=j)\\ -n_1\left(\frac{\nu}{1-\nu}\right)s\beta_{1i}\sum_{j=1}^{N}A_{ij}; & (i\neq j)\end{cases},\quad d^{62}_{ij}=\begin{cases} -n_1\left(\frac{\nu}{1-\nu}\right)\frac{s\beta_{1i}}{\eta_i}; & (i=j)\\ 0; & (i\neq j)\end{cases}$$

$$d^{63}_{ij}=\begin{cases} -\frac{1-2\nu}{2(1-2\nu)}s^2\beta^2_{1i}\left[A^{(2)}_{ii}+\left(2\beta_{2i}+\frac{1}{\eta_i}\right)A_{ii}+\left(\beta_{3i}+\frac{\beta_{2i}}{\eta_i}\right)\right]; & (i=j)\\ -\left(\frac{1-2\nu}{2(1-2\nu)}\right)s^2\beta^2_{1i}\left[\sum_{j=1}^{N}A^{(2)}_{ij}+\left(2\beta_{2i}+\frac{1}{\eta_i}\right)\sum_{j=1}^{N}A_{ij}\right]; & (i\neq j)\end{cases}$$

$$d^{64}_{ij}=\begin{cases} -\frac{\nu}{(1-\nu)}s\beta_{1i}\left[A_{ii}+\left(\beta_{2i}+\frac{1}{\eta_i}\right)\right]; & (i=j)\\ -\frac{\nu}{(1-\nu)}s\beta_{1i}\sum_{j=1}^{N}A_{ij}; & (i\neq j)\end{cases},$$

$$d^{65}_{ij}=\begin{cases} -\frac{1}{2(1-\nu)}\frac{s\beta_{1i}}{\eta_i}; & (i=j)\\ 0; & (i\neq j)\end{cases},\quad d^{66}_{ij}=\begin{cases} -n_1; & (i=j)\\ 0; & (i\neq j)\end{cases}$$

Elements of the temperature coefficients matrix of the ith sampling point are

$$\mathcal{G}_i = \begin{bmatrix} \mathbf{0}_{N\times N} & \mathbf{0}_{N\times N} & \mathbf{0}_{N\times N} & \mathbf{I}_{N\times N} & \mathbf{0}_{N\times N} & \mathbf{0}_{N\times N} \\ \mathbf{0}_{N\times N} & \mathbf{0}_{N\times N} & \mathbf{0}_{N\times N} & \mathbf{0}_{N\times N} & \mathbf{I}_{N\times N} & \mathbf{0}_{N\times N} \\ \mathbf{0}_{N\times N} & \mathbf{0}_{N\times N} & \mathbf{0}_{N\times N} & \mathbf{0}_{N\times N} & \mathbf{0}_{N\times N} & \mathbf{I}_{N\times N} \\ \mathbf{0}_{N\times N} & \mathbf{0}_{N\times N} & \mathbf{0}_{N\times N} & \mathbf{0}_{N\times N} & \mathbf{0}_{N\times N} & \mathbf{0}_{N\times N} \\ \mathbf{0}_{N\times N} & \mathbf{0}_{N\times N} & \mathbf{0}_{N\times N} & \mathbf{0}_{N\times N} & \mathbf{0}_{N\times N} & \mathbf{0}_{N\times N} \\ \mathbf{b}^{61}_{N\times N} & \mathbf{0}_{N\times N} & \mathbf{0}_{N\times N} & \mathbf{0}_{N\times N} & \mathbf{0}_{N\times N} & \mathbf{B}^{66}_{N\times N} \end{bmatrix}_{6N\times 6N} \tag{A.3}$$

where

$$b^{61}_{ij} = \begin{cases} \dfrac{(n_1+n_2)(1+\nu)}{1-\nu}\dfrac{\alpha|_{\xi=0}}{\alpha_1}; & (i=j) \\ 0; & (i\neq j) \end{cases}$$
$$b^{66}_{ij} = \begin{cases} \dfrac{1+\nu}{1-\nu}\dfrac{\alpha|_{\xi=0}}{\alpha_1}; & (i=j) \\ 0; & (i\neq j) \end{cases} \tag{A.4}$$

REFERENCES

[1] X.Y. Li, P.D. Li, G.Z. Kang, D.Z. Pan, Axisymmetric thermo-elasticity field in a functionally graded circular plate of transversely isotropic material, Mathematics and Mechanics of Solids 18 (5) (2012) 464–475.

[2] Y. Wang, R.Q. Xu, H.J. Ding, Analytical solutions of functionally graded piezo-electric circular plates subjected to axisymmetric loads, Acta Mechanica 215 (1–4) (2010) 287–305.

[3] X.Y. Li, H.J. Ding, W.Q. Chen, P.D. Li, Three-dimensional piezoelectricity solutions for uniformly loaded circular plates of functionally graded piezoelectric materials with transverse isotropy, ASME Journal of Applied Mechanics 80 (4) (2013) 041007, 12 pp..

[4] G.J. Nie, R.C. Batra, Stress analysis and material tailoring in isotropic linear thermoelastic incompressible functionally graded rotating disks of variable thickness, Composite Structures 92 (2010) 720–729.

[5] X.L. Peng, X.F. Li, Thermal stress in rotating functionally graded hollow circular disks, Composite Structures 92 (2010) 1896–1904.

[6] A. Hassani, M.H. Hojjati, G. Farrahi, R.A. Alashti, Semi-exact elastic solutions for thermo-mechanical analysis of functionally graded rotating disks, Composite Structures 93 (2011) 3239–3251.

[7] M. Bayat, B.B. Sahari, M. Saleem, A. Ali, S.V. Wong, Thermoelastic solution of a functionally graded variable thickness rotating disk with bending based on the first-order shear deformation theory, Thin-Walled Structures 47 (2009) 568–582.

[8] O. Sepahi, M.R. Forouzan, P. Malekzadeh, Large deflection analysis of thermo-mechanical loaded annular FGM plates on nonlinear elastic foundation via DQM, Composite Structures 92 (2010) 2369–2378.

[9] M.E. Golmakani, M. Kadkhodayan, Large deflection analysis of circular and annular FGM plates under thermo-mechanical loadings with temperature-dependent properties, Composites Part B: Engineering 42 (2011) 614–625.

[10] M.E. Golmakani, M. Kadkhodayan, An investigation into the thermoelastic analysis of circular and annular functionally graded material plates, Mechanics of Advanced Materials and Structures 211 (2014) 1–13.

[11] M. Shariyat, M.M. Alipour, A novel shear correction factor for stress and modal analyses of annular FGM plates with non-uniform inclined tractions and non-uniform elastic foundations, International Journal of Mechanical Sciences 87 (2014) 60–71.

[12] M.M. Alipour, M. Shariyat, Analytical zigzag-elasticity transient and forced dynamic stress and displacement response prediction of the annular FGM sandwich plates, Composite Structures 106 (2013) 426–445.

[13] M. Shariyat, M.M. Alipour, Semi-analytical consistent zigzag-elasticity formulations with implicit layerwise shear correction factors for dynamic stress analysis of sandwich circular plates with FGM layers, Composites Part B: Engineering 49 (2013) 43–64.

[14] Y. Wang, R.Q. Xu, H.J. Ding, Three-dimensional solution of axisymmetric bending of functionally graded circular plates, Composite Structures 92 (7) (2010) 1683–1693.

[15] M. Shariyat, R. Mohammadjani, Three-dimensional compatible finite element stress analysis of spinning two-directional FGM annular plates and disks with load and elastic foundation non-uniformities, Latin American Journal of Solids and Structures 10 (5) (2013) 859–890.

[16] M. Shariyat, R. Mohammadjani, Three-dimensional stress field analysis of rotating thick bidirectional functionally graded axisymmetric annular plates with nonuniform loads and elastic foundations, Journal of Composite Materials 48 (23) (2014) 2879–2904.

[17] A. Behravan Rad, Semi-analytical solution for functionally graded solid circular and annular plates resting on elastic foundations subjected to axisymmetric transverse loading, Advances in Applied Mathematics and Mechanics 4 (2012) 205–222.

[18] A. Behravan Rad, A. Alibeigloo, Semi-analytical solution for the static analysis of 2D functionally graded circular and annular circular plates resting on elastic foundation, Mechanics of Advanced Materials and Structures 20 (7) (2013) 515–528.

[19] A. Behravan Rad, Static response of 2-D functionally graded circular plate with gradient thickness and elastic foundations to compound loads, Structural Engineering and Mechanics 44 (2012) 139–161.

[20] A. Behravan Rad, M. Shariyat, A three-dimensional elasticity solution for two-directional FGM annular plates with non-uniform elastic foundations subjected to normal and shear tractions, Acta Mechanica Solida Sinica 26 (6) (2013) 671–690.

[21] E. Pan, Exact solution for simply supported and multilayered magneto-electric-elastic plates, ASME Journal of Applied Mechanics 68 (2001) 608–618.

[22] J.G. Wang, L.F. Chen, S.S. Fang, State vector approach to analysis of multilayered magneto-electroelastic plates, International Journal of Solids and Structures 40 (2003) 1669–1680.

[23] R.G. Lage, C.M.M. Soares, C.A.M. Soares, J.N. Reddy, Layerwise partial mixed finite element analysis of magneto-electro-elastic plates, Computers & Structures 82 (2004) 1293–1301.

[24] A. Alaimo, I. Benedetti, A. Milazzo, A finite element formulation for large deflection of multilayered magneto-electro-elastic plates, Composite Structures 107 (2014) 643–653.

[25] S. Razavi, A. Shooshtari, Nonlinear free vibration of magneto-electro-elastic rectangular plates, Composite Structures 119 (2015) 377–384.

[26] R.K. Bhangale, N. Ganesan, Static analysis of simply supported functionally graded and layered magneto-electro-elastic plates, International Journal of Solids and Structures 43 (2006) 3230–3253.

[27] E. Pan, F. Han, Exact solution for functionally graded and layered magneto-electro-elastic plates, International Journal of Engineering Science 43 (2005) 321–339.

[28] C. Jiangyi, C. Hualing, P. Ernian, Free vibration of functionally graded, magneto-electro-elastic, and multilayered plates, Acta Mechanica Solida Sinica 19 (2) (2006) 160–166.

[29] X.Y. Li, H.J. Ding, W.Q. Chen, Three-dimensional analytical solution for functionally graded magneto-electro-elastic circular plates subjected to uniform load, Composite Structures 83 (2008) 381–390.
[30] H.-L. Dai, T. Dai, L. Yang, Free vibration of a FGPM circular plate placed in a uniform magnetic field, Meccanica 48 (2013) 2339–2347.
[31] A. Behravan Rad, M. Shariyat, Three-dimensional magneto-elastic analysis of asymmetric variable thickness porous FGM circular plates with non-uniform tractions and Kerr elastic foundations, Composite Structures 125 (2015) 558–574.
[32] A. Ghorbanpour Arani, Z. Khoddami Maraghi, M.R. Mozdianfard, A.R. Shajari, Thermo-piezo-magneto-mechanical stresses analysis of FGPM hollow rotating thin disk, International Journal of Mechanics and Materials 6 (2010) 341–349.
[33] A.M. Zenkour, On the magneto-thermo-elastic responses of FG annular sandwich disks, International Journal of Engineering Science 75 (2014) 54–66.
[34] X.Y. Li, Y.H. Dong, C. Liu, Y. Liu, C.J. Wang, T.F. Shi, Axisymmetric thermo-magneto-electro-elastic field in a heterogeneous circular plate subjected to a uniform thermal load, International Journal of Mechanical Sciences 88 (2014) 71–81.
[35] A.C. Ugural, S.K. Fenster, Advanced Strength and Applied Elasticity, fourth ed., Printice Hall, New Jersey, 2003.
[36] E.M. Purcell, D.J. Morin, Electricity and Magnetism, third ed., Harvard University, Massachusetts, 2013.
[37] I.A. Abbas, A.M. Zenkour, LS model on electro-magneto-thermoelastic response of an infinite functionally graded cylinder, Composite Structures 96 (2013) 89–96.
[38] C. Shu, Differential Quadrature and its Application in Engineering, Springer, New York, 2000.
[39] F. Tornabene, A. Liverani, G. Caligiana, Laminated composite rectangular and annular plates: a GDQ solution for static analysis with a posteriori shear and normal stress recovery, Composites Part B: Engineering 43 (4) (2012) 1847–1872.
[40] A.J.M. Ferreira, E. Carrera, M. Cinefra, E. Viola, F. Tornabene, N. Fantuzzi, A.M. Zenkour, Analysis of thick isotropic and cross-ply laminated plates by generalized differential quadrature method and a Unified Formulation, Composites Part B: Engineering 58 (2014) 544–552.
[41] G.J. Nie, Z. Zhong, Semi-analytical solution for three-dimensional vibration of functionally graded circular plates, Computer Methods in Applied Mechanics and Engineering 196 (2007) 4901–4910.